



Research paper

Vicinal diaryl azole-based urea derivatives as potential cholesterol lowering agents acting through inhibition of SOAT enzymes



Palash Pal, Hardik P. Gandhi, Ashish M. Kanhed, Nirali R. Patel, Niraj N. Mankadia, Satish N. Baldha, Mahesh A. Barmade, Prashant R. Murumkar, Mange Ram Yadav*

Faculty of Pharmacy, Kalabhavan Campus, The Maharaja Sayajirao University of Baroda, Vadodra, 390001, India

ARTICLE INFO

Article history:

Received 23 September 2016

Received in revised form

13 February 2017

Accepted 14 February 2017

Available online 20 February 2017

Keywords:

Atherosclerosis

Cholesterol lowering agents

SOAT inhibitors

Vicinal diaryl compounds

ABSTRACT

A novel series of vicinal diaryl azole-urea derivatives were synthesized and evaluated for their potential to inhibit SOAT enzyme. Among the reported compounds, compound (**12d**) emerged as the most potent compound with an IC₅₀ value of 2.43 μM. In polaxamer-407 induced lipoprotein lipase inhibition model, compound (**12d**) reduced triglyceride turnover *in vivo*. Compound (**12d**) also showed dose-dependent prevention of serum total cholesterol and prevention of LDL-C elevation at a dose of 30 mg/kg. Furthermore, compound (**12d**) showed potential to stop falling levels of serum HDL-C dose-dependently and improved the atherogenic index. Effect of **12d** on body weight, plaque formation and development of atherogenic lesions were studied. Toxicological study of compound (**12d**) indicated that at a dose of 2000 mg/kg, **12d** was devoid of any signs of toxicity or mortality.

© 2017 Elsevier Masson SAS. All rights reserved.

1. Introduction

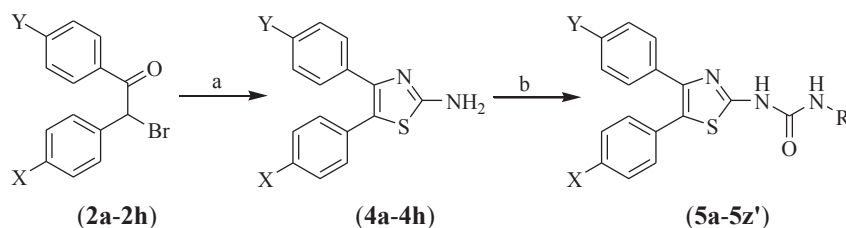
Cardiovascular diseases (CVD), a leading cause of deaths among the human population arises due to high serum cholesterol levels [1,2]. Other important risk factors include obesity, diabetes, hypertension, cigarette smoking (traditional and electronic) and lack of physical activity. Atherosclerosis is a CVD characterized by formation of lipid-rich plaques in the inner walls of arteries. Chronic hypercholesterolemia predisposes an individual towards the development of atherosclerosis [2]. Technically, the entire process is a remodeling event in the inner walls of medium and large arteries that leads to subendothelial deposition of fatty substances [3]. The end result of such a process is formation of thick, mature and obstructive plaque. Rupturing of the plaque leads to hemorrhage and formation of emboli or thrombosis at the site of the lesion [4]. Occlusion of the vessels may lead to myocardial infarction [5], the main cause of morbidity and mortality in the affected persons.

Cholesterol is a vital constituent required by the human body for the viability of all types of cells [6]. However, excess of the cholesterol is toxic to the cells causing cell death [7]. Formation of cholesterol esters as neutral lipids is imperative to the transport

and storage of cholesterol in plasma and steroidogenic tissues like the adrenals [8]. Cholesterol levels in the body are governed by various factors such as absorption of dietary cholesterol, *in situ* cholesterol synthesis and biliary cholesterol excretion [5]. Several therapeutic agents have been developed for lowering of lipid levels [9,10a] which are in current use. These include two novel PCSK9 (proprotein convertase subtilisin/kexin type 9) inhibitors approved in 2015 [10b]. Given the limitations of various lipid-lowering agents such as statins, fibrates and bile acid sequestrants, the search for novel lipid lowering agents still continues. There is a need for the development of non-statin based cholesterol lowering agents due to occurrence of/or concerns regarding adverse effects of statins. The adverse effects associated with statins include, but are not limited to, induction of diabetes mellitus, interstitial lung disease, hemorrhagic stroke, decreased cognition, tendon rupture and muscle-related symptoms. Muscle symptoms and tendinopathy are the most common adverse effects of statins. Muscle symptoms leading to elevation of creatine kinase (CK) levels upto 10 times the upper limit of normal levels are serious concerns that frequently lead to discontinuation of medication mandating the need for alternative therapies. Another problem is that all patients do not respond similarly to statins [10c]. Patients intolerant to statins or those not responding adequately may need to switch to alternative therapies to manage dyslipidemia and prevent atherosclerosis [10d].

* Corresponding author.

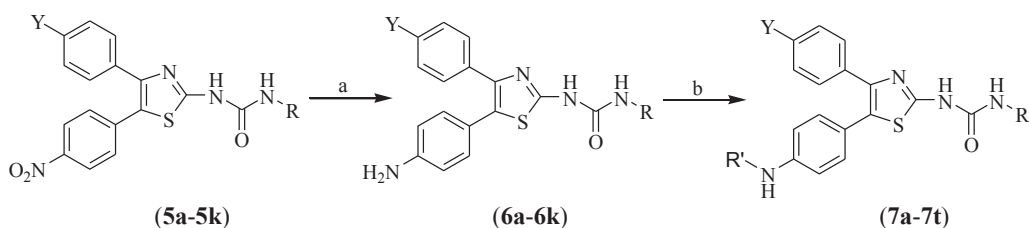
E-mail address: mryadav11@yahoo.co.in (M.R. Yadav).



Comp.	X	Y	Comp.	X	Y
(2a, 4a)	NO ₂	Me	(2e, 4e)	Cl	Me
(2b, 4b)	NO ₂	F	(2f, 4f)	Cl	F
(2c, 4c)	NO ₂	Cl	(2g, 4g)	Cl	OMe
(2d, 4d)	NO ₂	OMe	(2h, 4h)	H	H

Scheme 2. Synthesis of 2-thiazolyurea derivatives (5a-5z').

Reagents and conditions: (a) Thiourea, EtOH, reflux; (b) R-NCO, toluene, reflux.



Comp.	Y	R	Comp.	Y	R
(5a, 6a)	Me	2,4-F ₂ Ph	(5g, 6g)	Cl	<i>n</i> .Butyl
(5b, 6b)	Me	2,6-(Et) ₂ Ph	(5h, 6h)	Cl	<i>n</i> .Dodecyl
(5c, 6c)	Me	<i>n</i> .Butyl	(5i, 6i)	OMe	2,4-F ₂ Ph
(5d, 6d)	F	2,4-F ₂ Ph	(5j, 6j)	OMe	<i>n</i> .Butyl
(5e, 6e)	F	<i>n</i> .Butyl	(5k, 6k)	OMe	<i>n</i> .Heptyl
(5f, 6f)	Cl	2,4-F ₂ Ph			

Scheme 3. Synthesis of derivatives (7a-7t).

Reagents and conditions: (a) Fe powder, NaCl solution, MeOH, reflux; (b) (i) Acetic anhydride or mesyl chloride, THF or (ii) Isopropyl bromide/*n*.dodecyl bromide, K₂CO₃, DMF.

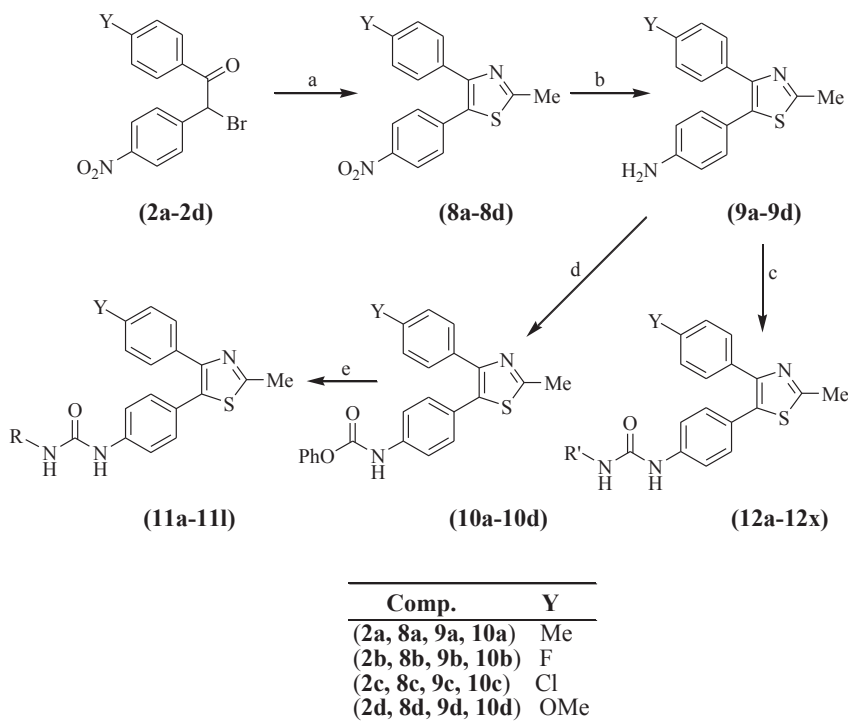
and oxadiazoles, the required starting derivatives were prepared using Scheme 1. The 1,2-diarylethanones (**1a-1h**) were prepared by Friedal-Craft acylation of the suitably substituted benzenes with the required phenylacetyl chloride derivatives. The ethanones (**1a-1h**) were either brominated to the desired bromo derivatives (**2a-2h**) or oxidized to the benzil derivatives (**3a-3c**) using selenium dioxide in DMSO [30a,b].

To prepare the 2-ureathiazoles (**5a-5z'**), Scheme 2 was followed. To construct the thiazole ring, the 2-bromoethanones (**2a-2h**) were reacted with thiourea to obtain the 2-aminothiazole derivatives (**4a-4h**) which when reacted with the desired type of isocyanates, the required urea derivatives (**5a-5z'**) were obtained. ¹H NMR spectra of a representative compound (**5t**) offered signals at δ 10.59 (bs, 1H, NH), 8.85 (bs, 1H, NH), 7.49–7.47 (d, 2H, Ar-H), 7.43–7.24 (m, 8H, Ar-H), 7.04–7.00 (t, 1H, Ar-H), 6.85–6.83 (d, 2H, Ar-H) and 3.77 (s, 3H, OCH₃).

The nitro group in compounds (**5a-5k**) was reduced to the basic amino group by reduction with iron powder. The resulting amino derivatives (**6a-6k**) were reacted with acetyl chloride/methanesulfonyl chloride or alkyl halides to obtain acidic or basic lipophilic functionalities in compounds (**7a-7t**) (Scheme 3). ¹H NMR spectra of compound (**7o**) offered signals at δ 10.63 (bs, 1H, NH), 6.66–8.22 (m, 11H, Ar-H), 3.79 (s, 3H, OCH₃), 3.57–3.79 (m, 1H, NHCH) and 1.22–1.24 (d, 6H, CH₃).

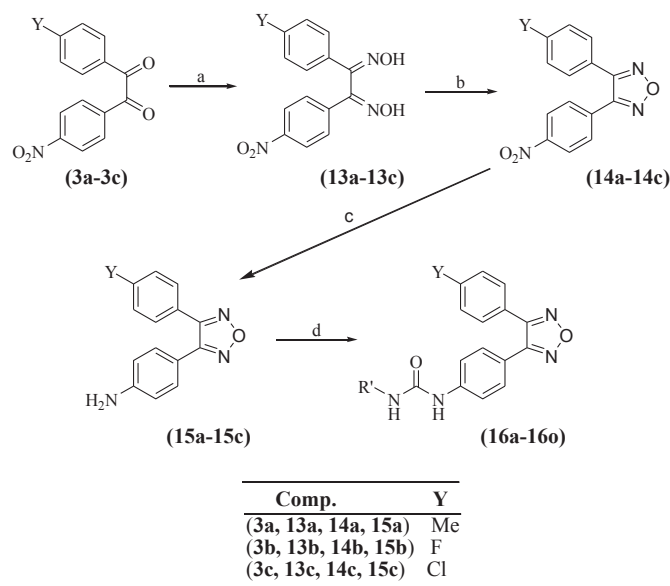
To Shift the urea functionality from the second position of the thiazole to the para position of the 5-phenyl ring, two different approaches were utilized (Scheme 4). The bromoethanones (**2a-2d**) were reacted with thioacetamide to yield the 2-methylthiazoles (**8a-8d**). Reduction of the 4-nitro group of these derivatives offered the amines (**9a-9d**). In one approach, the amines (**9a-9d**) on direct reaction with the desired isocyanates offered the targeted urea derivatives (**12a-12x**). In the second approach, the amines (**9a-9d**) were first reacted with phenyl chloroformate to obtain phenyl carbamates (**10a-10d**), which were further reacted with the required amines to obtain the desired 1,2-disubstituted urea derivatives (**11a-11l**). ¹H NMR spectrum of a representative compound (**11d**) showed signals at δ 6.94–7.50 (m, 11H, Ar-H), 6.06 (s, 1H, NH), 5.97 (s, 1H, NH), 3.31–3.34 (m, 2H, diisopropyl-CH), 2.82 (s, 3H, CH₃), 1.21–1.35 (m, 12H, diisopropyl-CH₃). Among the directly synthesized urea derivatives from the desired isocyanates the most potent compound (**12d**) offered proton signals at δ 7.12–7.40 (m, 8H, Ar-H), 6.59 (bs, 1H, NH), 4.82 (bs, 1H, NH), 3.21–3.3(q, 2H, NHCH₂), 2.72 (s, 3H, thiazole-CH₃), 2.32 (s, 3H, Ar-CH₃), 1.45–1.52 (m, 2H, CH₂), 1.32–1.41(m, 2H, CH₂) and 0.91–0.95 (t, 3H, CH₃) in its ¹H NMR spectrum.

For the synthesis of the oxadiazole derivatives, benzils (**3a-3c**) as the starting materials were oximated using hydroxylamine hydrochloride in a basic solvent like pyridine. The dioximes (**13a-13c**)



Scheme 4. Synthesis of compounds (11a-11l and 12a-12x).

Reagents and conditions: (a) Thioacetamide, MeOH, reflux; (b) Fe powder, NaCl solution, MeOH, reflux; (c) *R*-NCO, toluene, rt. (d) Phenyl chloroformate, THF, 0 °C; (e) *R*-NH₂, DMAP, DMF.



Scheme 5. Synthesis of oxadiazole derivatives (16a-16o).

Reagents and conditions: (a) Hydroxylamine HCl, pyridine, reflux; (b) Succinic anhydride, 180 °C; (c) Fe powder, NaCl solution, MeOH, reflux; (d) *R*-NCO, toluene, rt.

so obtained were dehydrated using succinic anhydride to obtain the oxadiazoles (**14a-14c**). The nitro group in these derivatives (**14a-14c**) was reduced and the resulting amino derivatives (**15a-15c**) were reacted with the required isocyanates to obtain the targeted 1,2-disubstituted urea derivatives (**16a-16o**) having oxadiazole ring in place of the thiazole ring system (Scheme 5). Compound (**16h**), a representative compound among the

oxadiazole series (**16a-16o**), offered signals at δ 8.41 (bs, 1H, NH), 7.21–7.61 (m, 8H, Ar-H), 5.91 (bs, 1H, NH), 3.62–3.81 (m, 2H, NHCH₂), 2.61–2.67 (m, 4H, CH₂), 1.2–1.4 (t, 3H, CH₃) in its proton NMR spectrum.

2.2. Biological

2.2.1. In vitro SOAT inhibition assay of the test compounds

The synthesized compounds were evaluated for their potential to inhibit SOAT activity *in vitro* using rat microsomal SOAT. The test compounds were evaluated at a fixed concentration (10 μ M) for pan-SOAT activity as per the reported method [31] and were not evaluated for activity against individual isoforms. The results of this preliminary screening are depicted in Tables 1–4. The preliminary screening data showed that several of these compounds exhibited good inhibition (some of them \geq 60% at 10 μ M concentration) which was comparable to that of the standard pan-SOAT inhibitor avasimibe (**1**). This data was used further to select potent compounds for determination of their IC₅₀ values. A threshold value of 35% inhibition was chosen arbitrarily and all those compounds showing a minimum of 35% inhibition of microsomal SOAT activity were selected for IC₅₀ determination at five different concentrations. Since it was also aimed to develop a credible 3D-QSAR model to validate the pharmacophore models for the compounds reported in this paper, some compounds with lower inhibition values were also chosen for their IC₅₀ determinations, as inclusion of full spectrum of low to high potency compounds was a basic requirement for developing a good 3D-QSAR. The IC₅₀ values are depicted in Table S3, Supplementary material.

Looking at the contents of these tables (Tables 1–4), it could be inferred that placing the urea moiety at the 4th position of the 5-phenyl ring (Table- 3) was best suited for good SOAT inhibitory activity and it offered more number of potent compounds as compared to the 2-ureidothiazole (Tables 1 and 2) analogs.

Table 1
The synthesized urea derivatives (**5a–5z'**) and their *in vitro* SOAT enzyme inhibitory activity.

Comp.	X	Y	R	% Inhibition (at 10 μ M conc)	Comp.	X	Y	R	% Inhibition (at 10 μ M conc)
(5a)	NO ₂	Me	2,4-F ₂ Ph	3.86	(5o)	Cl	Me	n.Butyl	36.37
(5b)	NO ₂	Me	2,6-(Et) ₂ Ph	1.03	(5p)	Cl	F	2,4-F ₂ Ph	42.34
(5c)	NO ₂	Me	n.Butyl	3.86	(5q)	Cl	F	2,6-(Et) ₂ Ph	1.58
(5d)	NO ₂	F	2,4-F ₂ Ph	3.59	(5r)	Cl	F	n.Butyl	3.30
(5e)	NO ₂	F	n.Butyl	2.98	(5s)	Cl	F	n.Dodecyl	1.91
(5f)	NO ₂	Cl	2,4-F ₂ Ph	3.28	(5t)	Cl	OMe	Ph	56.86
(5g)	NO ₂	Cl	n.Butyl	3.02	(5u)	Cl	OMe	2,4-F ₂ Ph	2.98
(5h)	NO ₂	Cl	n.Dodecyl	1.77	(5v)	Cl	OMe	n.Butyl	27.58
(5i)	NO ₂	OMe	2,4-F ₂ Ph	3.40	(5w)	Cl	OMe	n.Heptyl	1.73
(5j)	NO ₂	OMe	n.Butyl	3.12	(5x)	H	H	Ph	10.56
(5k)	NO ₂	OMe	n.Heptyl	1.52	(5y)	H	H	2,4-F ₂ Ph	3.03
(5l)	Cl	Me	Ph	9.58	(5z)	H	H	n.Butyl	2.56
(5m)	Cl	Me	2,4-F ₂ Ph	3.93	(5z')	H	H	n.Dodecyl	1.20
(5n)	Cl	Me	2,6-(Et) ₂ Ph	1.52					

Table 2
The prepared urea derivatives (**7a–7t**) and their *in vitro* SOAT enzyme inhibitory activity.

Comp.	Y	R'	R	% Inhibition (at 10 μ M conc)	Comp.	Y	R'	R	% Inhibition (at 10 μ M conc)
(7a)	Me	COMe	2,4-F ₂ Ph	3.06	(7k)	Cl	COMe	n.Butyl	3.75
(7b)	Me	SO ₂ Me	2,4-F ₂ Ph	2.17	(7l)	Cl	SO ₂ Me	n.Butyl	5.63
(7c)	Me	COMe	n.Butyl	5.23	(7m)	OMe	COMe	2,4-F ₂ Ph	38.98
(7d)	Me	SO ₂ Me	n.Butyl	32.67	(7n)	OMe	SO ₂ Me	2,4-F ₂ Ph	19.63
(7e)	F	COMe	2,4-F ₂ Ph	23.32	(7o)	OMe	i.Pr	2,4-F ₂ Ph	51.73
(7f)	F	SO ₂ Me	2,4-F ₂ Ph	18.9	(7p)	OMe	n.Dodecyl	2,4-F ₂ Ph	1.77
(7g)	F	COMe	n.Butyl	15.4	(7q)	OMe	COMe	n.Butyl	39.45
(7h)	F	SO ₂ Me	n.Butyl	0.43	(7r)	OMe	SO ₂ Me	n.Butyl	5.45
(7i)	Cl	COMe	2,4-F ₂ Ph	2.03	(7s)	OMe	i.Pr	n.Butyl	4.67
(7j)	Cl	SO ₂ Me	2,4-F ₂ Ph	6.39	(7t)	OMe	n.Dodecyl	n.Butyl	3.36

Table 3
The phenylurea derivatives (**11a–11l** and **12a–12x**) and their *in vitro* SOAT enzyme inhibitory activity.

Comp.	Y	R	% Inhibition (at 10 μ M conc)	Comp.	Y	R	% Inhibition (at 10 μ M conc)
(11a)	Me	2,6-(i.Pr) ₂ Ph	11.19	(11g)	Cl	2,6-(i.Pr) ₂ Ph	12.64
(11b)	Me	3,4,5-(OMe) ₃ Ph	21.88	(11h)	Cl	3,4,5-(OMe) ₃ Ph	24.44
(11c)	Me	Morpholinoethyl	18.96	(11i)	Cl	Morpholinoethyl	12.31
(11d)	F	2,6-(i.Pr) ₂ Ph	42.12	(11j)	OMe	2,6-(i.Pr) ₂ Ph	30.13
(11e)	F	3,4,5-(OMe) ₃ Ph	41.98	(11k)	OMe	3,4,5-(OMe) ₃ Ph	25.44
(11f)	F	Morpholinoethyl	29.32	(11l)	OMe	Morpholinoethyl	21.46
Comp.	Y	R'	% Inhibition (at 10 μ M conc)	Comp.	Y	R'	% Inhibition (at 10 μ M conc)
(12a)	Me	Ph	13.36	(12m)	Cl	Ph	6.88
(12b)	Me	2,4-F ₂ Ph	26.63	(12n)	Cl	2,4-F ₂ Ph	1.3
(12c)	Me	2,6-(Et) ₂ Ph	30.94	(12o)	Cl	2,6-(Et) ₂ Ph	63.32
(12d)	Me	n.Butyl	64.91	(12p)	Cl	n.Butyl	60.71
(12e)	Me	n.Heptyl	33.41	(12q)	Cl	n.Heptyl	52.18
(12f)	Me	n.Dodecyl	46.19	(12r)	Cl	n.Dodecyl	5.75
(12g)	F	Ph	16.81	(12s)	OMe	Ph	11.37
(12h)	F	2,4-F ₂ Ph	4.97	(12t)	OMe	2,4-F ₂ Ph	22.27
(12i)	F	2,6-(Et) ₂ Ph	46.68	(12u)	OMe	2,6-(Et) ₂ Ph	31.62
(12j)	F	n.Butyl	59.91	(12v)	OMe	n.Butyl	40.02
(12k)	F	n.Heptyl	62.96	(12w)	OMe	n.Heptyl	22.21
(12l)	F	n.Dodecyl	34.47	(12x)	OMe	n.Dodecyl	27.52

Comparing the activities of the compounds obtained from the thiazole and the oxadiazole ring systems, it became clear that thiazole ring was better suited to SOAT inhibition than the oxadiazole ring (Table 4) because the thiazole ring yielded more number of compounds with higher potency.

Apart from the fact that 2-ureidothiazole scaffold offered low to medium active compounds, aryl substituents as R on the urea

moiety and methoxy group (Y) on the phenyl ring offered more potent compounds (**5t**, **7m**, **7o**, **7q**). Polar groups like amino group on the other phenyl ring (**6b**) offered low potency compound. Substituting an acetyl/methanesulfonyl or an alkyl on the amino group did not improve the activity profile of the resulting compounds beyond a certain point.

In the 2-methylthiazole series having the substituted urea

Table 4
In vitro SOAT enzyme inhibitory activity of compounds (**16a–16o**).

Comp.	Y	R'	% Inhibition (at 10 μ M conc)	Comp.	Y	R'	% Inhibition (at 10 μ M conc)
(16a)	Me	2,4-F ₂ Ph	13.52	(16i)	F	<i>n</i> .Heptyl	30.93
(16b)	Me	2,6-(Et) ₂ Ph	0.34	(16j)	F	<i>n</i> .Dodecyl	50.07
(16c)	Me	<i>n</i> .Butyl	2.83	(16k)	Cl	2,4-F ₂ Ph	21.23
(16d)	Me	<i>n</i> .Heptyl	18.65	(16l)	Cl	2,6-(Et) ₂ Ph	8.25
(16e)	Me	<i>n</i> .Dodecyl	9.15	(16m)	Cl	<i>n</i> .Butyl	23.03
(16f)	F	2,4-F ₂ Ph	47.06	(16n)	Cl	<i>n</i> .Heptyl	4.3
(16g)	F	2,6-(Et) ₂ Ph	44.85	(16o)	Cl	<i>n</i> .Dodecyl	18.51
(16h)	F	<i>n</i> .Butyl	54.5				

moiety attached to the para position of the 5-phenyl ring (compounds **11** and **12**), non-polar and bulky groups are preferred at both the positions (Y and R'; **11d**, **12d**, **12f**, **12i–12k**, **12o–12q**). Polar groups like morpholinoethyl (at R' position) or methoxy (at Y position) are not preferred for higher potency. Methyl or chloro groups at position Y, and *n*.butyl, *n*.heptyl or 2,6-diethylphenyl groups at R' position yielded the most potent compounds. Compound (**12d**) with a combination of methyl at Y position and *n*.butyl at R' position was found out to be the most potent compound (IC₅₀ 2.43 μ M) with SOAT inhibition activity which was better than the standard drug avasimibe (**1**; IC₅₀ 4.01 μ M).

In the oxadiazole series (compounds **16**), the most potent compounds were observed to have fluoro group at position Y. Bulky lipophilic groups like 2,6-diethylphenyl, *n*.butyl, *n*.dodecyl or 2,4-difluorophenyl at R' position offered more potent compounds than the rest in the series.

It can be summarized that thiazole ring is better suited to SOAT inhibitory activity over the oxadiazole ring and the urea moiety should not be directly linked to the thiazole ring system in the vicinal diarylthiazoles. On the contrary, the urea moiety should be attached to one of the phenyl rings and the substituents on the urea moiety and the other phenyl ring should be bulky and nonpolar in nature for obtaining potent SOAT inhibitors.

Several urea-based compounds reported in the literature have been reported to show good microsomal SOAT inhibitory activity. These reported compounds are usually di- or tri-substituted urea derivatives with an array of substituents on either sides of the urea moiety. Several researchers have reported SAR studies of their own di-substituted urea derivatives showing promising *in vitro* SOAT inhibition and good anti-hypercholesterolemic activity. These compounds were found to exhibit [32–36] microsomal SOAT inhibition (IC₅₀) in the range of 0.007–5.3 μ M. These activities

seemed promising and comparable to the standard inhibitors of SOAT like avasimibe and pactimibe but majority of these compounds were retracted from further perusal due to prevalence of different types of problems with them [32,34,37,38].

The compounds reported in this paper are all di-substituted urea derivatives. Altering the basic scaffold by exchanging heteroaryl moieties i.e., thiazole/oxadiazole in place of imidazole, and altering the substituent pattern have been tried in this study to generate a range of novel compounds which offered some potent SOAT inhibitors. As is evident from the results (Table S3, Supplementary material), compounds (**12d**, **12i**, **12k**, **12o**, **12p** and **12q**) were the most potent inhibitors, comparable in activity to the standard avasimibe (**1**) [39]. Considering their *in vitro* potency it was planned to evaluate these compounds further in some *in vivo* animal model(s).

2.3. Poloxamer-407 induced lipoprotein lipase inhibition model for evaluating potent compounds

Increase in triglyceride production rates has been observed after inhibition of plasma lipoprotein lipase causing temporal changes in plasma triglyceride (TG) levels [40–42]. Poloxamer-407 or P-407 (Pluronic® F-125), a non-ionic detergent was found to be an inhibitor of lipoprotein lipase. It has been reported [43,44] that known inhibitors of SOAT prevent the cholesteryl ester input in plasma and reduce hepatic TG secretion rate. Fig. 1 shows the effects of the selected compounds (**12d**, **12i**, **12k**, **12o**, **12p** and **12q**) on TG turnover following P-407 administration. In commensurate with the *in vitro* data, compound (**12d**) was found to be the most active compound in this *in vivo* model also, amongst the selected lot. Administration of compound (**12d**) caused only moderate changes in TG turnover (~20 fold) over a period of 24 h. Similar

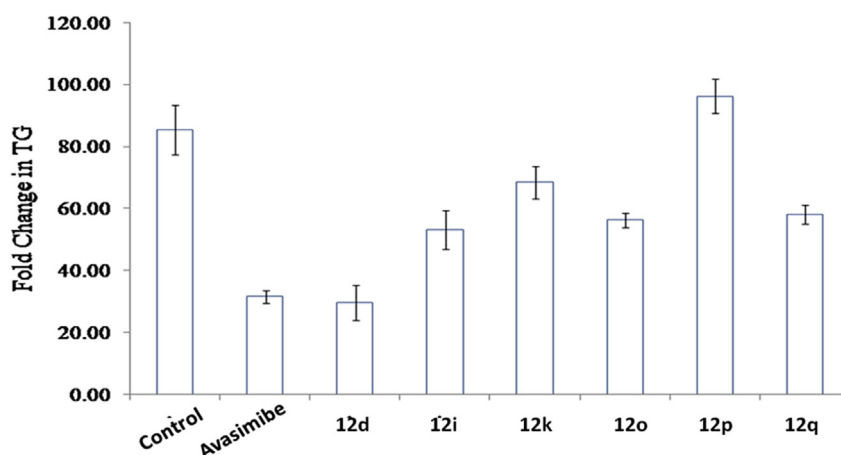


Fig. 1. Effects of test compounds and standard drug on 24 h triglyceride turnover measured as fold-change in TG at 0 h and 24 h after administration of P-407.

effect was also observed in the avasimibe-treated group. While the control group animals showed a mean 80-fold change in base-line TG levels, the other derivatives showed 50–90 fold changes in TG turnover. This experiment revealed that there could be a correlation between SOAT inhibition and TG turnover as avasimibe was also found to be active against TG turnover mediated through LPL inhibition. It is known [45] that chylomicrons, which form a significant chunk of TG, after losing triacylglycerols acquire cholesteryl esters from the lipoproteins. Since administration of SOAT inhibitors can prevent *de Novo* formation of cholesteryl esters, the pool of cholesteryl esters that remains available for acquisition to chylomicrons is depleted. This biochemical inhibition thus correlates well with the observations of the present study where administration of SOAT inhibitors like avasimibe and the test compound (**12d**) resulted in reduced TG turnover *in vivo*.

2.4. Evaluation of compound (**12d**) in animal models of diet-induced atherogenesis

2.4.1. Effects on serum lipids and lipoproteins

An animal model of diet-induced atherogenesis in rats has been reported [46] to be a valid model for the study of compounds effective against atherosclerosis. It was decided to observe the effect of compound (**12d**) on serum levels of lipids and lipoproteins in diet-induced atherogenesis in rats.

Before the initiation of the study, the mean cholesterol values for all the animals were found to average around 91.16 ± 4.54 mg/dl. It was observed that cholesterol levels started rising dramatically after about 2-weeks of the initiation of high cholesterol diet (HCD)

and kept on rising towards the terminal stage of the study in the progression control group. A dose-dependent prevention of serum total cholesterol elevation was observed in the groups (Fig. 2) that were co-administered compound (**12d**). A dose of 10 mg/kg was not found to be significant in preventing cholesterol elevation but the higher dose (30 mg/kg) group showed a dramatic prevention ($P < 0.01$) of cholesterol elevation with serum total cholesterol levels remaining constant at 138 ± 9.50 mg/dl at the end of the study. On the contrary as expected, HDL-C values in the control group showed a downward trend as the study progressed and a 2-fold reduction in serum HDL-C levels was observed at the end of the study. Treatment with compound (**12d**) was able to stop the falling levels of HDL-C dose-dependently in the treated animals (Fig. 2). SOAT inhibition causes significant changes in availability of cholesterol pools. This leads to mobilization of intracellular cholesterol from the SOAT-available compartment to that of apolipoprotein-mediated HDL assembly. This could be the possible mechanism by which **12d** prevented a decline in HDL-C levels [46b]. Minor elevations in triglyceride levels between the initial and final stages of the study were observed but the changes were not statistically significant (P value 0.251).

Analysis of lipoprotein cholesterol levels (LDL-C and VLDL-C) were based on the Friedewald's formula [47a] which showed that VLDL-C elevations were not significant among the treated groups (Fig. 3a). However, a sharp rise in LDL-C (more than 12-fold) was observed in the progression control group ($P < 0.001$). The test compound-treated lower dose (10 mg/kg) group showed only modest prevention in LDL-C elevation but the higher dose (30 mg/kg) treated group indicated a significant prevention ($P < 0.001$;

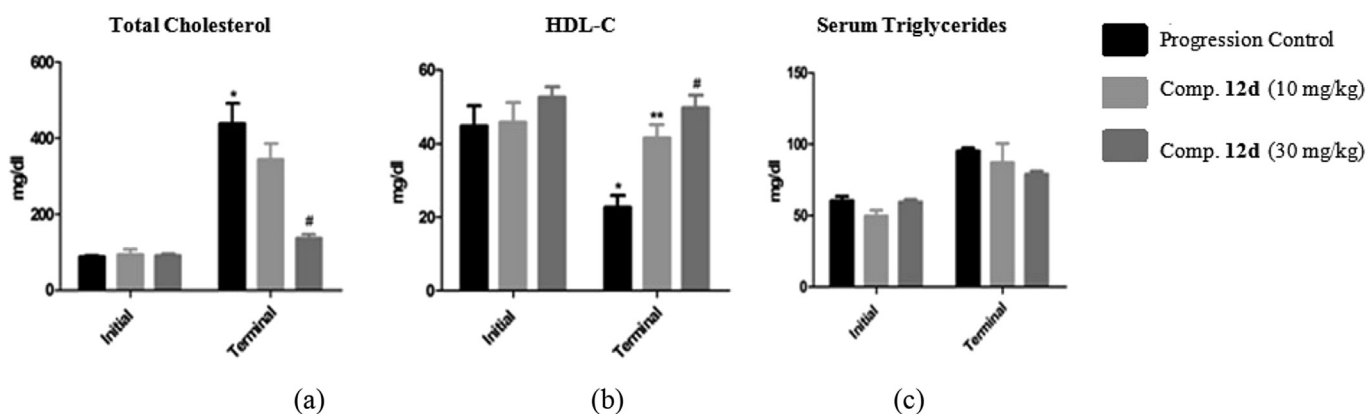


Fig. 2. Effect of compound (**12d**) on (a) Total cholesterol; (b) HDL levels; (c) Triglycerides.

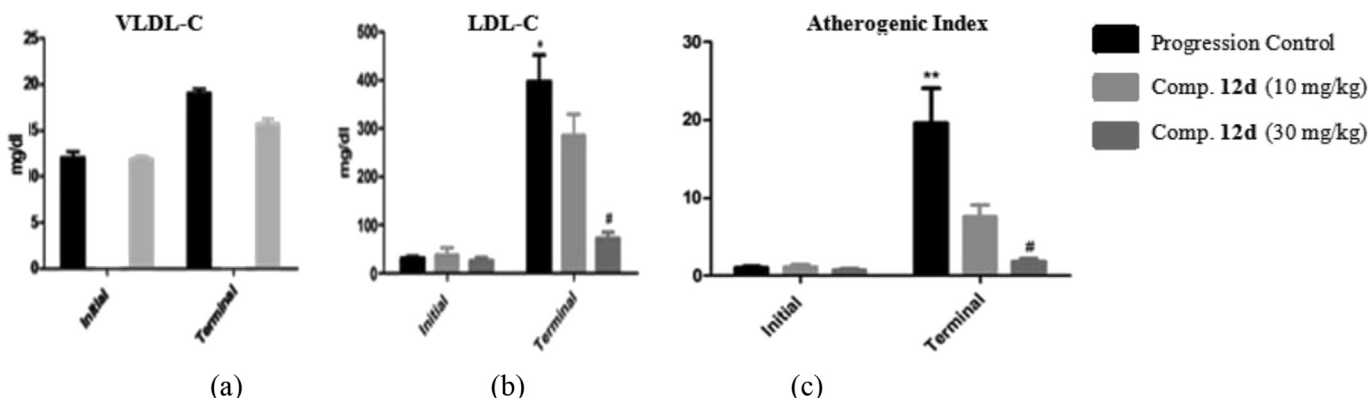


Fig. 3. Effects of compound (**12d**) on (a) VLDL-C, (b) LDL levels, (c) Atherogenic index.

Fig. 3b) of LDL-C elevation as compared to the progression control group.

Atherogenic index, a surrogate marker of coronary artery disease, is determined by ratio of triglycerides to HDL [47b]. The atherogenic index indicated the prevalence of non-HDL cholesterol over HDL-C. This data indicated that after 8 weeks of administration of HCD, the atherogenic index peaked to 19.59 ± 5.8 in the control group animals. Such a high value of the atherogenic index indicated that the animals were prone to the development of atherosclerotic lesions. Co-administration of compound (**12d**) in the diet reduced the atherogenic index to 7.55 ± 0.9 and 1.82 ± 0.34 respectively in the 10 mg/kg and 30 mg/kg treated groups (Fig. 3c).

2.5. Effect of compound (**12d**) on body weight

The curve of body weight remained relatively unaffected over the whole treatment period for all the groups. No significant changes in body weights of the animals were observed between the final and initial stages of the study. At the end of the study there was no significant difference between the progression control (290.3 ± 8.1 g) and the test compound (**12d**) treated groups at doses of 10 mg/kg (294 ± 14.3 g) and 30 mg/kg (299 ± 6.6 g). We hypothesize that SOAT inhibition-mediated cholesterol reduction might lead to hyperphagic response owing to modulation of leptin levels on chronic therapy. This mechanism might be responsible for maintaining the body weight in spite of significant cholesterol reduction. Fig. 4 shows the difference in body weights among the groups.

Based on these results it was decided to evaluate compound (**12d**) in an atherosclerosis model because the test compound (**12d**) also showed favorable effect on serum triglycerides apart from microsomal SOAT inhibition.

2.6. Effect of compound (**12d**) on lipid accumulation lesion area in the aortae

Lesion area in the aortic strips were characterized by *en face* lipid staining with Sudan red IV. Photographs of pinned aortae upon area analysis by ImageJ revealed that $22.35 \pm 7.9\%$ area from the progression control group was stained as compared to the $16.21 \pm 1.07\%$ ($P > 0.05$) in the lower dose (10 mg/kg) treated-group and $8.42 \pm 2.7\%$ ($P < 0.05$) in the higher dose (30 mg/kg) treated group (Fig. 5). The results indicate that treatment with 30 mg/kg of compound (**12d**) shows nearly 3-fold reduction in the lesion area. Representative images of the aortae are shown in Fig. 6.

Accumulation of lipids in the intimal was indicated by the formation of fatty streaks in the aortic strips which got stained in maroon color with Sudan red IV. These types of streaks are evident along the length of the aorta of the control group animals. Some

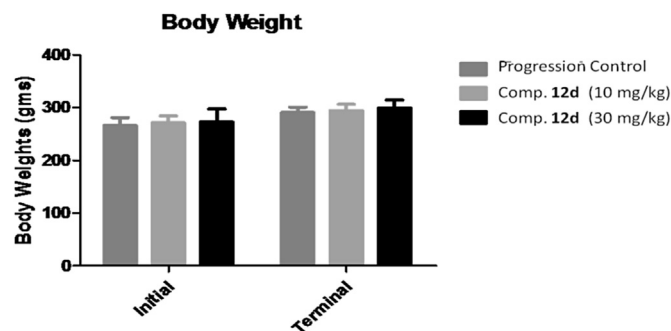


Fig. 4. Effect on body weights of groups.

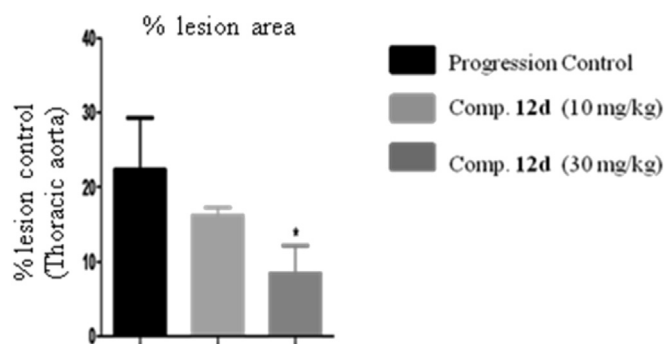


Fig. 5. Lipid accumulation lesion area in the aortae.

intermittent fatty streaks are evident in aorta of the lower dose (10 mg/kg) treated (with compound **12**) animals. Absence of such fatty streaks could be seen in the aorta of animals treated with the higher dose (30 mg/kg) of the test compound (**12d**). These observations are indicative of the atheroprotective role of compound (**12d**).

Based on the results of *in vivo* evaluation studies of compound (**12d**), it was concluded that the test compound (**12d**) possessed significantly high potential in modulating the pathological development of atherosclerotic lesions positively.

2.7. Effect of compound (**12d**) on luminal lipid plaque formation

Luminal plaque formation in the control and test compound treated groups was studied by taking multiple sections of the aortae and then staining them with Sudan Red IV to stain the lipid core of the plaque. Representative images from different groups are shown in Fig. 7. The images indicate that long-term consumption of atherogenic diet has led to the development of a plaque core which obscured the lumen of the aortic root (also known as aortic sinus). Aortic root is the most putative site for the formation of lipid-rich plaques, although a plaque may be formed in any anatomical region of the artery. Such observations of thickened intima in progression control groups have been reported [48]. No evidence for the development of lipid-rich cores was found in the test compound (**12d**)-treated animals.

It is worthy to mention here that the protective effects of compound (**12d**) reported in this study were obtained without any evidence of cutaneous or adrenal toxicities, which are the commonly reported serious side effects of SOAT inhibitors [48–50].

2.8. Toxicological evaluation of compound (**12d**)

2.8.1. Single dose acute oral toxicity

Earlier studies on different urea-based derivatives have shown fatal toxicities of the test compounds upto the doses of 2000 mg/kg [49,50]. Some compounds have been reported to exhibit adrenal toxicity at high doses which could be an indication of non-specific cytotoxicity [37,51]. To ensure the safety of the test compound (**12d**), it was administered at 2000 mg/kg to a group of animals. The post-treatment examination period was 14 days from the date of dosing the animals. Body weights of the animals were recorded on days 0, 7 and 14. Slight fluctuations were observed in the body weight of the animals during the observation period. The animals were closely watched during the first 6 h of dosing. The animals were starved during this period with free access to water. No significant changes were recorded during this period. This part coincided with the light cycle and most of the animals were asleep. When awake, the animals showed normal grooming behavior and

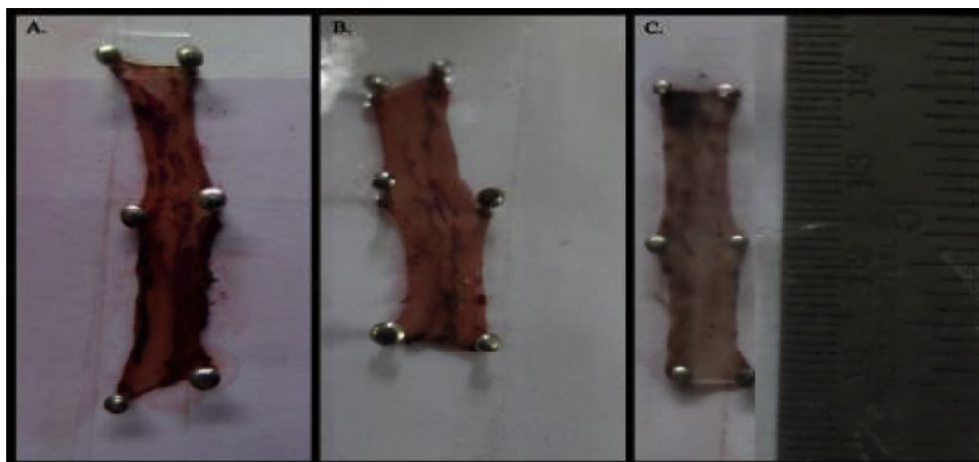


Fig. 6. Accumulation of intimal lipids in control and compound (**12d**) treated groups. Formation of fatty streaks in progression control group (A); in test compound treated group at a dose of 10 mg/kg (B); at dose of 30 mg/kg (C).

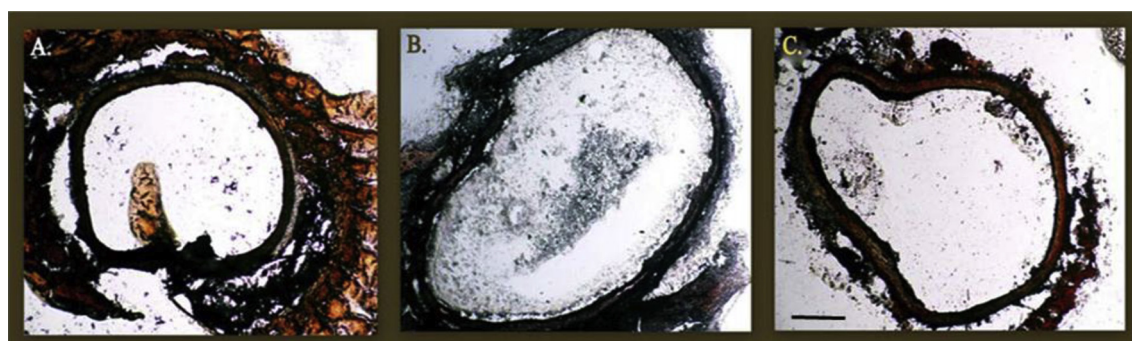


Fig. 7. Cross-sectional areas from aortic roots after sacrificing animals of different groups. Streaks in the intimal area were not observed in any group but development of plaque was evident in the HCD progression control (A). Minor damage to the arterial wall was evident in the region where plaque development was initiated. Intimal linings appear normal and there was no evidence of diameter obscuration in the treated group (B and C). The scale bar in figure C represents 500 μm .

the water intake was also normal. During the entire post-treatment observation period, special attention was paid to observe alteration of skin color or fur, abnormal locomotion or breathing and changes in the eyes. No untoward observations were made in this regard till the terminal day of the study. No mortality was observed till day 14. At the end of the study period, the animals were euthanized and major organs like brain, heart, lung, liver, kidney, spleen and adrenals were harvested. Gross necropsy was performed by an individual blinded to the groups. No macroscopic lesions were observed. Viscera, gastrointestinal tract and mucus of the lungs appeared normal. Adrenal glands exhibited normal shape and size and any signs of shrinkage were absent.

Administration of 2000 mg/kg of the test compound (**12d**) showed no signs of toxicity or mortality during the test period. The LD_{50} of compound (**12d**) in rats was thus found to be > 2000 mg/kg.

2.9. Repeat dose oral toxicity

Repeat dose toxicity study for 28 days at 60 mg/kg oral dose of compound (**12d**) was performed on rats. No untoward observations were made regarding body weight, food intake or normal behavior at the end of the study. The most common side effect related to the mechanism of action of SOAT inhibitors upon repeated dose administration is cutaneous xanthomatosis [48,52,53]. This effect was not evident in any of the subjects under study even after an extended period of 14-days of the study. Biochemical estimates did

not suggest any major digression from normal values. Urinary output and hematological data appeared normal.

It was concluded from this study that repeat dose oral administration of the test compound (**12d**) at a dose of 60 mg/kg was safe.

2.10. Computational studies

All members of MBOAT family have several transmembrane domains and majority of them possess two conserved residues which may be the active-site residues, a conserved histidine (His) embedded in a hydrophobic stretch of residues and an asparagine (Asn) or histidine within a more hydrophilic region, some 30–50 residues upstream [24,54]. Till date the 3D structures of SOAT-1 and SOAT-2 isoforms have not been reported. As there is no homologous protein present for the conserved part of SOAT, it is very difficult to generate the 3D structure of SOAT. So, it was planned to generate a 3D structure of the conserved part of SOAT using *de novo* protein modeling. These generated protein models were compared with the results obtained from pharmacophore and docking studies. With the help of NCBI Blast, the MBOAT conserved region of the isoform SOAT-1 (amino acids 286 to 520) has been identified which represents the functional unit of the target protein (Fig. S1, supplementary material).

The obtained sequence was submitted to I-TASSER (Iterative Threading ASSEMBLY Refinement) [55–57], a hierarchical method for prediction of the protein structure and function. In this method

the structural templates are initially identified from the PDB by multiple threading approach LOMETS (Local Meta-Threading-Server) which is a locally installed PDB library for meta-threading approach having multiple threading programs in I-TASSER server. Templates of the highest significance in the threading alignments were identified using LOMETS by measuring the Z-score (Table S1, supplementary material).

After the threading alignment, thousands of conformations (called decoys) were generated and to finalize the model, SPICKER program was used in I-TASSER to cluster all the decoys based on the pair-wise structure similarity, and report up to five models, which corresponded to the five largest structure clusters. From these models the confidence of each model was quantitatively measured by C-score. With the best C-Score model, TM-align program was used to match it with all the structures in PDB. From the TM-align, top ten proteins with the maximum structural similarities to the predicted I-TASSER model were obtained (Table S2, supplementary material).

As the highest matching model **4cadC** represents the integral membrane protease Rce1 and our target SOAT-1 is also a membrane bound protein, Model1 was selected for determining the 3D structure of MBOAT conserved domain of the SOAT-1.

As the isoforms 1 and 2 are having almost 55% overall sequence identity and more than 60% MBOAT sequence identity, the 3D-structure of SOAT-2 was developed using MBOAT sequence (Fig. S2, supplementary material) and the developed SOAT-1 model as the template structure in MODELLER, with the help of homology modeling. As the probable active site residues His-460 for SOAT-1 and His-434 for SOAT-2 had been reported, these were used to identify the active sites in both of the developed receptor models.

The pharmacophore and 3D-QSAR models for SOAT inhibitors were developed using our own 32 test compounds reported in this paper as SOAT inhibitors by using PHASE module of Schrodinger.

The SOAT inhibitory activity in IC_{50} (M) was converted into $1/\log IC_{50}$ values (pIC_{50}) which was used as the biological activity parameter for the development of the pharmacophore model (Table S3, supplementary material).

PHASE [58] employs tree-based partitioning algorithm and detects thoroughly the spatial arrangements of functional groups that are common and necessary for the biological activity for a set of high-affinity ligands. The data set having 32 molecules was divided into a training set containing 26 molecules and test set having 6 compounds for the development of 3D-QSAR models. For the distribution of dataset into training and test set, structural diversity over the full range of activity was considered and the models were developed.

With a prerequisite that all active compounds should match all the features, five featured common pharmacophore hypotheses were developed from different variants by means of a tree-based partition algorithm. These generated hypotheses were assessed on the basis of 'Survival' and 'Survival-inactive' scores. The best model was found to be linked with the five-point hypothesis having a hydrogen bond acceptor group, a hydrogen bond donor group, a hydrophobic group and two aromatic rings (ADHRR). The inter-site distances and angles in the pharmacophoric features were aligned on the best fit compound which also happened to be the most active compound (**12d**, Fig. S3, supplementary material). The graph for actual versus predicted activity of training set and test set are shown in Fig. S4 (supplementary material). To evaluate the predictive ability of the model, the test set compounds were used. Based on the R^2 , Q^2 , SD, RMSE and Pearson-R values, the developed 3D-QSAR model was found to be predictive and accurate (results are shown in Table S4, supplementary material).

The volume occlusion maps obtained from 3D-QSAR model recognized the important features necessary for the ligand-

receptor interactions. The occlusion maps are represented by blue and red colors indicating favorable and unfavorable interactions respectively. The occlusion maps (donor, hydrophobic and electronegative) with the most active compound (**12d**) for the developed 3D-QSAR model are shown in Fig. S5A (supplementary material). As shown in Fig. S5A for the most active compound (**12d**), the blue regions are observed near the NH group of urea linker, explaining its high activity because of its hydrogen bond donating tendency. Lower potency of compounds (**11i** and **12h**) could also be explained very well because the urea NH moiety in these compounds was overlapping the non-favorable i.e. red region. In docking study of the most active compound (**12d**) the said NH moiety was observed to be oriented towards the $-CONH_2$ of Asn421 of SOAT1, while in SOAT2 the same group appeared towards C=O group of Leu275 and Val398; whereas in the less potent compound like (**11i**), this was not the case and the change in orientation was mainly observed because of the morpholine group which was separated from the urea moiety by an ethylene linker. Fig. S5B shows the hydrophobic volume occlusion map. Here, the high activity of **12d** could be explained pretty well, as the alkyl (methyl) and the aromatic groups were in blue regions causing possible hydrophobic interactions. The binding affinity of **12d** to the enzyme is further strengthened by π - π stacking of the thiazole ring with His460 and by hydrophobic interactions of the aromatic rings with Phe453, Phe486 and Trp499 of SOAT1. In SOAT2 model the hydrophobic interactions of the said groups are observed with Val406, Phe427, His434, Met463 and Trp473 residues of the enzyme. The urea group was seen in the red region exhibiting hydrophilic interactions. This observation was supported by the docking study as the said urea group was observed to be placed in an area covered by polar regions of Val424 and Asn421 of SOAT1, and in case of SOAT2 the polar groups of Val398 supported similar observations. Deviations from favorable interactions were observed in case of a majority of the less active compounds. Low activity of compound (**12s**) could be explained as most of the hydrophobic groups in the ligand were oriented into the red regions. High activity of **12d** was further proved by the presence of carbonyl and thiazole ring-N in the blue regions, as seen in the electronegative maps (Fig. S5C, supplementary material).

Apart from the 3D-QSAR validation parameters, other widely reported statistical validation techniques were also applied [59,60]. To derive these statistical results, data set was divided into two sets. Compounds with pIC_{50} 4.9 and above were considered as 'active' and those with activity below this value were considered as 'inactive', and modified R^2 i.e. (R^2_m), sensitivity, specificity, accuracy, precision and Matthew's correlation coefficient (MCC) were calculated (results are shown in Table S5, supplementary material).

Further, docking of the most active ligand (**12d**) was done on the predicted active sites of SOAT1 and SOAT2. Results of the docking studies further validated existence of pharmacophoric features projected in the generated pharmacophore models. The binding patterns of the most active compound (**12d**) with SOAT-1 and SOAT-2 are shown in Fig. 8 and Fig. 9 respectively. The active compound (**12d**) shows almost similar affinity to the proposed active site residues of both the isoforms. The docking score for compound (**12d**) with SOAT-1 was -6.15 , whereas it was observed to be -6.67 with SOAT-2. In SOAT-1 the test compound (**12d**) interacts mostly by van der Waals or hydrophobic interactions. The thiazole ring forms π - π stacking with His460, whereas the two aromatic rings show hydrophobic interactions with Asn421, Phe453 and Trp499. In addition to these interactions the butyl chain fits into the hydrophobic pocket of Leu304, Ile377, Thr380, Phe381 and Tyr417. While in case of SOAT-2 the proposed active site residue His343 shows strong π - π interaction with the *p*-methyl phenyl ring attached to the thiazole ring. The thiazole ring and the

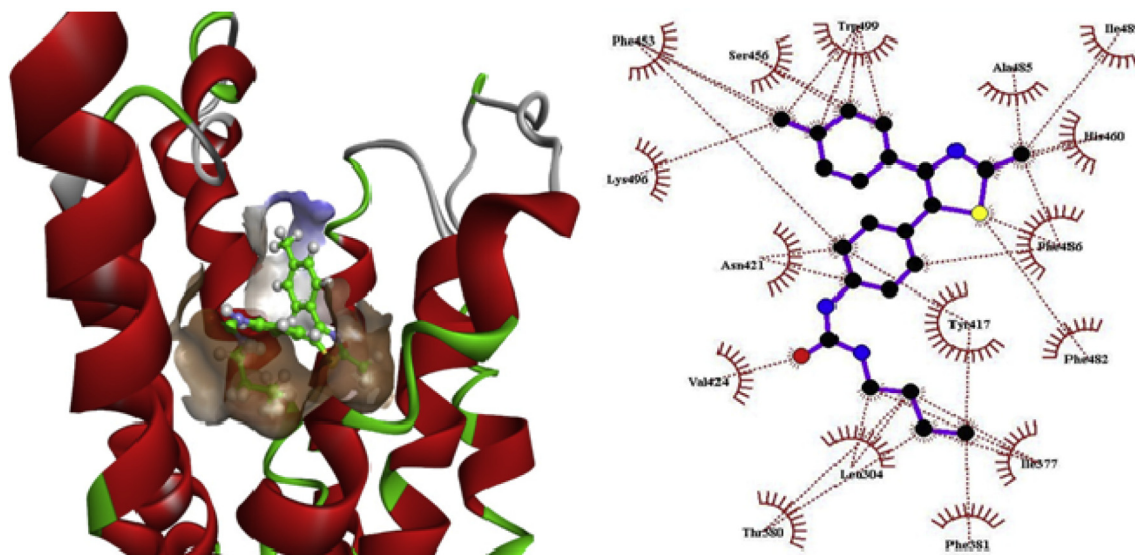


Fig. 8. Docking of the most active compound (**12d**) in the active site of the proposed SOAT-1 model.

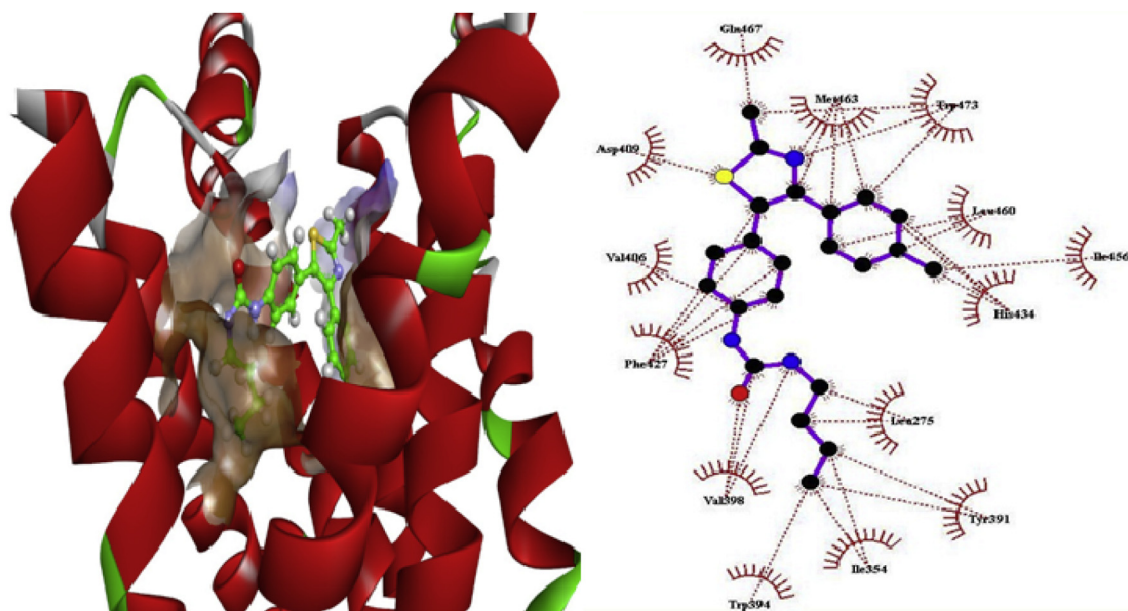


Fig. 9. Docking of the most active compound (**12d**) in the active site of the of proposed SOAT-2 model.

two aromatic rings attached to the thiazole ring are observed to be stabilized by hydrophobic interactions with Val406, Asp409, Phe427, Ile456, Leu460, Met463, Gln467 and Trp473. The butyl chain is strongly stabilized by hydrophobic part of Leu275, Ile354, Tyr391, Trp394 and Val398. In **11i**, a less potent compound, the morpholine ring of the compound possessing higher topological polar surface area and poor lipophilicity appears in the polar region of the target protein as a complimentary region for interaction hence, it should be better stabilized. But, in docking studies with SOAT1, this group was observed to be surrounded by more nonpolar amino acid residues like Leu275, Ile301, Ile354 and Trp394, supporting the observed poor activity of compound (**11i**). In SOAT2, the same group was observed to be surrounded by amino acids Leu275 and Trp394.

This pharmacophore based 3D-QSAR study and the accompanying docking study based on the proposed 3D models of SOAT-1

and SOAT-2 enzymes could prove to be of immense help for the development of novel potent SOAT inhibitors.

3. Conclusion

Novel series of vicinal diaryl thiazole- and oxadiazole-based urea derivatives have been synthesized and evaluated for their SOAT inhibitory activity. To get structural insights for SOAT inhibitory activity, the urea group was attached to different positions of the scaffold in the synthesized molecules i.e. directly to the azole ring and then to one of the phenyl rings. All of the synthesized compounds were evaluated for their *in vitro* SOAT inhibitory activity. Based on the data obtained from the preliminary biological evaluation it was concluded that the thiazole containing compounds were more potent than the oxadiazoles as exemplified by compound (**12d**). As far as the safety of compound (**12d**) was

concerned, it was found to be devoid of any adrenal or cutaneous toxicity in an animal model of chronic toxicity. Three dimensional structures of SOAT-1 and SOAT-2 enzymes were also developed by using homology modelling technique. Further, pharmacophore and 3D-QSAR models for SOAT inhibitors were also developed by using the compounds reported in the paper. The developed 3D-QSAR models were validated using different statistical methods. Docking study of the most active compound (**12d**) was performed in the predicted active sites of both the enzymes. Compound (**12d**) showed promising activity worthy of consideration for further studies for its development as a cholesterol lowering agent.

4. Experimental

4.1. Chemistry

All solvents and chemicals were purified before use. Melting points were determined on a Veego melting point apparatus and are uncorrected. The IR spectra were obtained (wave numbers in cm^{-1}) on Bruker ALPHA-T (Germany) FT-IR spectrophotometer using KBr discs. ^1H NMR and ^{13}C NMR spectra were recorded on a Bruker Advance-II 400 MHz spectrometer (some samples were run on 500 MHz spectrometer also) in CDCl_3 or DMSO- d_6 solvents. Chemical shifts are given in δ values (ppm) using tetramethylsilane (TMS) as the internal standard; coupling constants (J) are given in Hz. Signal multiplicities are characterized as s (singlet), d (doublet), t (triplet), q (quartet) and m (multiplet). Mass spectra were obtained on Thermo Fisher mass spectrometer with EI ion source. Elemental analyses were recorded on Thermo Fisher FLASH 2000 organic elemental analyzer. Merck F-254 commercial plates were used for analytical TLC to follow the course of reactions and check the product purity. Silica gel 60 (Merck, 300–400 mesh) was used for flash chromatography (CombiFlash RF 200, Teledyne ISCO). Structures of all the compounds were found to be consistent with their analytical and spectral data.

4.2. General procedure for the synthesis of 2-thiazolylurea derivatives (**5a–5z'**)

To a solution of compounds (**4a–4h**) (0.82 mM, 1 eq) in dry toluene (10 ml), the required isocyanates (1.60 mM, 2.0 eq) were added under nitrogen. The reaction mixture was stirred at room temperature for 4–5 h and monitored by TLC. The solid precipitate so obtained was filtered and washed with toluene to remove the excess isocyanate, dried and collected the products (**5a–5z'**) as such.

4.2.1. 1-Butyl-3-[5-(4-chlorophenyl)-4-(4-methylphenyl)thiazol-2-yl]urea (**5o**)

Prepared as per the general procedure using compound (**4e**) and *n*-butyl isocyanate to obtain the desired compound (**5o**). Yield 31%; mp = 181–183 °C; TLC R_f = 0.69 (*n*-Hexane: Ethyl acetate, 7:3); UV_{max} (MeOH): 242 nm; IR (KBr, cm^{-1}): 3410, 2929, 2869, 1698, 1534, 1444, 1295, 1241, 1092, 822; ^1H NMR: δ 11.34 (bs, 1H, NH), 6.9–7.4 (m, 8H, Ar-H), 2.8–2.9 (m, 2H, NHCH_2), 2.35 (s, 3H, Ar- CH_3), 1.16–1.25 (m, 4H, $-\text{CH}_2$), 0.82–0.90 (m, 3H, CH_3); ^{13}C NMR: δ 160.10, 153.03, 142.49, 137.40, 132.38, 130.46, 129.68, 129.41, 128.71, 127.99, 127.89, 122.48, 38.98, 30.73, 20.23, 18.19, 12.68; Anal. Calcd for $\text{C}_{21}\text{H}_{22}\text{ClN}_3\text{OS}$: C, 63.07; H, 5.54; N, 10.51. Found: C, 63.20; H, 5.35; N, 10.59.

4.2.2. 1-[5-(4-Chlorophenyl)-4-(4-fluorophenyl)thiazol-2-yl]-3-(2,4-difluorophenyl)urea (**5p**)

Prepared as per the general procedure using compound (**4f**) and 2,4-difluorophenyl isocyanate to obtain the desired compound (**5p**). Yield 37%; mp = 205–207 °C; TLC R_f = 0.51 (*n*-Hexane: Ethyl

acetate, 7:3); IR (KBr, cm^{-1}): 3416, 3118, 1720, 1610, 1564, 1505, 1432, 1297, 1198, 829; ^1H NMR: δ 10.71 (bs, 1H, NH), 8.83 (bs, 1H, NH), 8.07 (s, 1H, Ar-H), 6.82–7.40 (m, 10H, Ar-H); MS: m/z 459.9 $[\text{M}+1]^+$; Anal. Calcd for $\text{C}_{22}\text{H}_{13}\text{ClF}_3\text{N}_3\text{OS}$: C, 57.46; H, 2.85; N, 9.14. Found: C, 57.51; H, 2.76; N, 9.21.

4.2.3. 1-Butyl-3-[5-(4-chlorophenyl)-4-(4-methoxyphenyl)thiazol-2-yl]urea (**5v**)

Prepared as per the general procedure using compound (**4g**) and *n*-butyl isocyanate to obtain the desired compound (**5v**). Yield 55%; mp = 203–205 °C; TLC R_f = 0.58 (*n*-Hexane: Ethyl acetate, 7:3); UV_{max} (MeOH): 250.2 nm; IR (KBr, cm^{-1}): 3403, 2931, 1692, 1609, 1566, 1532, 1446, 1293, 1249, 1093, 831; ^1H NMR: δ 10.6 (bs, 1H, NH), 6.8–7.4 (m, 8H, Ar-H), 6.6 (bs, 1H, NH), 3.75 (s, 3H, OCH_3), 3.1 (m, 2H, NHCH_2), 1.39 (m, 2H, CH_2), 1.25 (m, 2H, CH_2), 0.92 (t, 3H, CH_3 , J = 7.2 Hz); MS: m/z 414.97 $[\text{M}^+]$; ^{13}C NMR: δ 158.67, 158.01, 153.90, 143.87, 131.98, 131.53, 130.57, 129.58, 128.71, 127.15, 120.93, 113.54, 54.93, 31.59, 19.44, 13.64, 13.56; Anal. Calcd for $\text{C}_{21}\text{H}_{22}\text{ClN}_3\text{O}_2\text{S}$: C, 60.64; H, 5.33; N, 10.10. Found: C, 60.76; H, 5.28; N, 10.23.

4.3. Synthesis of compounds (**7a–7t**)

4.3.1. 1-[5-(4-Acetamidophenyl)-4-(4-methylphenyl)thiazol-2-yl]-3-(2,4-difluorophenyl)urea (**7a**)

To a stirred solution of the amine (**6a**) (0.25 g, 1.02 mM) in THF (10 ml), acetic anhydride (0.12 ml, 1.02 mM) and a few drops of pyridine were added at 0–5 °C. The reaction mixture was stirred for 2 h at room temperature, poured into ice-cold water (50 ml) and the excess amount of pyridine was neutralized by addition of a few drops of dil HCl. The precipitate so formed was filtered, washed with water and dried. The crude product was purified by column chromatography using *n*-hexane/EtOAc as the mobile phase to obtain the pure product (**7a**). Yield 65%; mp = 260–262 °C; TLC R_f = 0.30 (*n*-Hexane: Ethyl acetate, 7:3); UV_{max} (MeOH): 245.20 nm; IR (KBr, cm^{-1}): 3415, 3126, 2962, 1702, 1666, 1615, 1554, 1401, 1288, 845; ^1H NMR: δ 9.78 (s, 1H, NH), 8.88 (s, 1H, NH), 8.09 (s, 1H, NH), 7.83 (s, 1H, Ar-H), 7.48–7.50 (m, 2H, Ar-H), 7.26–7.28 (m, 2H, Ar-H), 7.11–7.13 (m, 2H, Ar-H), 6.96–7.05 (m, 2H, Ar-H), 6.90–6.96 (m, 1H, Ar-H), 6.80–6.84 (m, 1H, Ar-H), 2.24 (s, 3H, COCH_3), 2.04 (s, 3H, Ar- CH_3); MS: m/z 478.7 $[\text{M}^+]$; Anal. Calcd for $\text{C}_{25}\text{H}_{20}\text{F}_2\text{N}_4\text{O}_2\text{S}$: C, 62.75; H, 4.21; N, 11.71. Found: C, 62.88; H, 4.07; N, 11.90.

4.3.2. 1-[5-(4-Acetamidophenyl)-4-(4-methoxyphenyl)thiazol-2-yl]-3-(2,4-difluorophenyl)urea (**7m**)

Prepared as per the procedure given under (**7a**). Yield 62%; mp = 160–162 °C; TLC R_f = 0.17 (*n*-Hexane: Ethyl acetate, 3:7); UV_{max} (MeOH): 253 nm; IR (KBr, cm^{-1}): 3406, 1675, 1610, 1615, 1548, 1512, 1403, 1293, 1253, 834; ^1H NMR: δ 9.87 (bs, 1H), 8.09 (bs, 1H), 6.74–8.15 (m, 11H), 3.73 (s, 3H), 2.04 (s, 3H); Anal. Calcd for $\text{C}_{25}\text{H}_{20}\text{F}_2\text{N}_4\text{O}_3\text{S}$: C, 60.72; H, 4.08; N, 11.33. Found: C, 60.85; H, 3.95; N, 11.39.

4.3.3. 1-[5-(4-Acetamidophenyl)-4-(4-methoxyphenyl)thiazol-2-yl]-3-butylurea (**7q**)

Prepared as per the procedure given under (**7a**). Yield 78%; mp = 168–170 °C; TLC R_f = 0.17 (*n*-Hexane: Ethyl acetate, 3:7); UV_{max} (MeOH): 251 nm; IR (KBr, cm^{-1}): 3405, 3247, 2953, 1668, 1529, 1402, 1248, 832; ^1H NMR: δ 7.5 (bs, 1H), 6.72–7.39 (m, 8H, Ar-H), 3.71 (s, 3H, OCH_3), 2.97–2.99 (m, 2H, NHCH_2), 2.10 (s, 3H, COCH_3), 1.41–1.26 (m, 4H, CH_2), 0.78–0.81 (t, 3H, CH_3); MS: m/z 438.8 $[\text{M}^+]$; Anal. Calcd for $\text{C}_{23}\text{H}_{26}\text{N}_4\text{O}_3\text{S}$: C, 62.99; H, 5.98; N, 12.78. Found: C, 63.12; H, 5.77; N, 12.91.

4.4. General procedure for the synthesis of compounds (11a–11l)

To a solution of compounds (10a–10d) (0.3 g, 0.45 mM) in DMF (5 ml), DMAP (0.26 g, 2.1 mM) and the desired amines (0.15 g, 0.85 mM) were added. The reaction mixture was stirred for 12 h at room temperature and monitored by TLC. The reaction mixture was poured into ice-cold water containing dil HCl. The precipitate so obtained was filtered off and purified by flash chromatography using dichloromethane: methanol as eluent to yield the desired derivatives (11a–11l).

4.4.1. 1-(3,4,5-Trimethoxyphenyl)-3-(4-(2-methyl-4-(4-fluorophenyl)thiazol-5-yl)phenyl)urea (11e)

Prepared as per the general procedure using compound (10b) and 3,4,5-trimethoxyaniline to obtain compound (11e). Yield 82%; mp = 224–226 °C; TLC R_f = 0.50 (*n*-Hexane: Ethyl acetate, 7:3); IR (KBr, cm⁻¹): 3268, 2961, 1703, 1600, 1540, 1507, 1410, 1321, 1207, 1128, 838; ¹H NMR: δ 8.89 (s, 1H, NH), 8.75 (s, 1H, NH), 6.80–7.50 (m, 10H, Ar-H), 3.78 (s, 6H, OCH₃), 3.66 (s, 3H, OCH₃), 2.71 (s, 3H, CH₃); Anal. Calcd for C₂₆H₂₄FN₃O₄S: C, 63.27; H, 4.90; N, 8.51. Found: C, 63.36; H, 4.82; N, 8.64.

4.4.2. 1-(2-(4-Morpholino)ethyl)-3-(4-(2-methyl-4-(4-fluorophenyl)thiazol-5-yl)phenyl)urea (11f)

Prepared as per the general procedure using compound (10b) and 4-(2-aminoethyl)morpholine to obtain the desired compound (11f). Yield 92%; mp = 179–181 °C; TLC R_f = 0.59 (Chloroform: MeOH, 5:1); IR (KBr, cm⁻¹): 3309, 2925, 1636, 1584, 1515, 1405, 1311, 1219, 1115, 836; ¹H NMR: δ 6.17 (s, 1H, NH), 6.93–7.49 (m, 8H, Ar-H), 3.87–3.89 (m, 4H, CH₂), 3.50–3.54 (m, 2H, CH₂), 2.81–2.84 (m, 6H, CH₂), 2.68 (s, 3H, thiazole-CH₃); Anal. Calcd for C₂₃H₂₅FN₄O₂S: C 62.71, H 5.72, N 12.72. Found: C, 62.89, H 5.69, N 12.87.

4.4.3. 1-(2,6-Diisopropylphenyl)-3-(4-(2-methyl-4-(4-methoxyphenyl)thiazol-5-yl)phenyl)urea (11j)

Prepared as per the general procedure using compound (10d) and 2,6-diisopropylaniline to obtain compound (11j). Yield 83%; mp = 200–202 °C; TLC R_f = 0.38 (*n*-Hexane: Ethyl acetate, 3:2); IR (KBr, cm⁻¹): 3294, 2962, 1651, 1593, 1549, 1401, 1310, 1248, 1177, 836; ¹H NMR: δ 8.81 (s, 1H, NH), 7.55 (s, 1H, NH), 7.40–7.44 (m, 4H, Ar-H), 7.25–7.12 (m, 5H, Ar-H), 6.83–6.81 (d, 2H, Ar-H), 3.77 (s, 3H, OCH₃), 3.17–3.24 (m, 2H, diisopropyl-CH), 2.68 (s, 3H, CH₃), 1.17–1.27 (m, 12H, diisopropyl-CH₃); Anal. Calcd for C₃₀H₃₃N₃O₂S: C, 72.11; H, 6.66; N, 8.41. Found: C, 72.19; H, 6.52; N, 8.49.

4.5. General procedure for the synthesis of compounds (12a–12x)

Compounds (12a–12x) were synthesized by adopting the procedure as described under compounds (7a–7t) using compounds (9a–9d) and the required isocyanates.

4.5.1. 1-Butyl-3-(4-(2-methyl-4-(4-fluorophenyl)thiazol-5-yl)phenyl)urea (12j)

Yield 63%; mp = 178–180 °C; TLC R_f = 0.35 (*n*-Hexane: Ethyl acetate, 7:3); UV_{max} (ACN): 248 nm; IR (KBr, cm⁻¹): 3314, 3117, 2962, 1634, 1585, 1514, 1403, 1310, 1224, 835; ¹H NMR: δ 8.32 (s, 1H, NH), 7.2–7.75 (m, 8H, Ar-H), 5.95 (bs, 1H, NH), 3.16–3.19 (m, 2H, NHCH₂, J = 6.6 Hz), 2.72 (s, 3H, thiazole-CH₃), 1.32–1.52 (m, 4H, CH₂), 0.91–0.95 (t, 3H, CH₃, J = 7.28); ¹³C NMR: δ 163.69, 163.51, 155.40, 138.81, 131.99, 131.05, 130.75, 130.67, 130.31, 126.61, 120.03, 115.36, 40.19, 32.16, 20.03, 19.17, 13.76; Anal. Calcd for C₂₁H₂₂FN₃O₂S: C, 65.77; H, 5.78; N, 10.96. Found: C, 65.83; H, 5.63; N, 11.09.

4.5.2. 1-Heptyl-3-(4-(2-methyl-4-(4-fluorophenyl)thiazol-5-yl)phenyl)urea (12k)

Yield 56%; mp = 154–156 °C; TLC R_f = 0.36 (*n*-Hexane: Ethyl acetate, 7:3); UV_{max} (ACN): 248.80 nm; IR (KBr, cm⁻¹): 3320, 2928, 1633, 1585, 1554, 1403, 1222, 836; ¹H NMR: δ 7.98 (bs, 1H, NH), 5.75 (s, 1H, NH), 6.88–7.55 (m, 8H, Ar-H), 3.12–3.32 (m, 2H, NHCH₂), 2.72 (s, 3H, thiazole-CH₃), 1.21–1.67 (m, 10H, CH₂), 0.92–0.95 (t, 3H, CH₃); ¹³C NMR: δ 163.67 (d, J = 80 Hz), 161.01, 156.22, 147.90, 139.25, 132.20, 131.06, 130.70 (d, J = 32 Hz), 130.11, 125.95, 119.47, 115.33 (d, J = 84 Hz), 40.29, 31.75, 30.15, 29.01, 26.88, 22.57, 19.10, 14.04; Anal. Calcd for C₂₄H₂₈FN₃O₂S: C, 67.74; H, 6.63; N, 9.87. Found: C, 67.87; H, 6.49; N, 10.14.

4.5.3. 1-(2,6-Diethylphenyl)-3-(4-(2-methyl-4-(4-chlorophenyl)thiazol-5-yl)phenyl)urea (12o)

Yield 43%; mp = 248–250 °C; TLC R_f = 0.72 (*n*-Hexane: Ethyl acetate, 8:2); UV_{max} (MeOH): 259.20 nm; IR (KBr, cm⁻¹): 3285, 2962, 1637, 1588, 1548, 1464, 1311, 1228, 829; ¹H NMR: δ 7.03–7.55 (m, 11H, Ar-H), 2.88–2.91 (q, 4H, CH₂), 1.19–1.23 (t, 6H, CH₃), 2.72 (s, 3H, thiazole-CH₃); ¹³C NMR: δ 163.85, 155.44, 147.85, 138.97, 133.46, 133.42, 132.62, 130.31, 130.24, 128.50, 126.39, 119.97, 20.04, 19.18, 13.78; MS: m/z 474.8 [M⁺]; Anal. Calcd for C₂₇H₂₄ClN₃O₂S: C, 68.12; H, 5.51; N, 8.83. Found: C, 67.98; H, 5.72; N, 8.95.

4.5.4. 1-Butyl-3-(4-(2-methyl-4-(4-chlorophenyl)thiazol-5-yl)phenyl)urea (12p)

Yield 63%; mp = 140–142 °C; TLC R_f = 0.35 (*n*-Hexane: Ethyl acetate, 8:2); UV_{max} (ACN): 252.40 nm; IR (KBr, cm⁻¹): 3326, 1636, 1585, 1560, 1490, 1349, 1229, 837; ¹H NMR: δ 8.31 (s, 1H, NH), 5.93 (s, 1H, NH), 7.13–7.66 (m, 8H, Ar-H), 3.17–3.24 (m, 2H, NHCH₂), 2.72 (s, 3H, thiazole-CH₃), 1.45–1.50 (m, 2H, CH₂), 1.32–1.41 (m, 2H, CH₂), 0.92–0.95 (t, 3H, CH₃, J = 7.2 Hz); ¹³C NMR: δ 162.63, 155.15, 146.49, 140.52, 133.36, 132.81, 132.33, 129.79, 129.41, 127.84, 123.45, 117.51, 31.31, 29.05, 26.42, 22.09, 18.70; Anal. Calcd for C₂₁H₂₂ClN₃O₂S: C, 63.07; H, 5.54; N, 10.51. Found: C, 63.29; H, 5.43; N, 10.67.

4.6. General procedure for the preparation of urea derivatives (16a–16o)

The urea derivatives (16a–16o) were prepared by reacting the amino derivatives (15a–15c) with the desired isocyanates by the procedure as reported for the preparation of compounds (5a–5z') to obtain the urea derivatives (16a–16o).

4.6.1. 1-(2,4-Difluorophenyl)-3-(4-(3-fluorophenyl)-1,2,5-oxadiazol-3-yl)phenyl)urea (16f)

Yield 68%; mp = 212–214 °C; TLC R_f = 0.32 (*n*-Hexane: Ethyl acetate, 8:2); IR (KBr, cm⁻¹): 3301, 3120, 3085, 1654, 1620, 1453, 1426, 1294, 1229, 1102, 848; ¹H NMR: δ 9.3 (bs, 1H, NH), 8.4 (bs, 1H, NH), 8.12–8.18 (m, 1H, Ar-H), 7.56–7.60 (m, 4H, Ar-H), 7.41–7.43 (m, 2H, Ar-H), 7.23–7.27 (m, 2H, Ar-H), 6.89–7.05 (m, 2H, Ar-H); Anal. Calcd for C₂₁H₁₃F₃N₄O₂: C, 61.47; H, 3.19; N, 13.65. Found: C, 61.76; H, 3.03; N, 13.73.

4.6.2. 1-(2,6-Diethylphenyl)-3-(4-(3-fluorophenyl)-1,2,5-oxadiazol-3-yl)phenyl)urea (16g)

Yield 73%; mp = 210–212 °C; TLC R_f = 0.35 (*n*-Hexane: Ethyl acetate, 8:2); IR (KBr, cm⁻¹): 3286, 2966, 1639, 1553, 1453, 1402, 1304, 1235, 841; ¹H NMR: δ 8.8 (s, 1H, NH), 7.10–7.51 (m, 11H, Ar-H), 7.0 (s, 1H, NH), 2.61–2.67 (q, 4H, CH₂), 1.2–1.4 (t, 6H, CH₃); Anal. Calcd for C₂₅H₂₃FN₄O₂: C, 69.75; H, 5.39; N, 13.02. Found: C, 69.88; H, 5.24; N, 13.15.

4.6.3. 1-(3-Heptyl)-3-(4-(3-fluorophenyl)-1,2,5-oxadiazol-3-yl)phenylurea (**16i**)

Yield 69%; mp = 136–138 °C; TLC R_f = 0.35 (*n*-Hexane: Ethyl acetate, 8:2); IR (KBr, cm^{-1}): 3365, 3132, 2927, 1647, 1570, 1401, 1310, 1255, 1096, 810; ^1H NMR: δ 8.41 (bs, 1H, NH), 7.0–7.5 (m, 8H, Ar-H), 5.91 (bs, 1H, NH), 3.37–3.45 (m, 2H, NHCH_2), 1.37–1.45 (m, 10H, CH_2), 0.9–1.01 (t, 3H, CH_3); ^{13}C NMR: δ 165.24, 162.74, 155.53, 155.52, 152.15, 141.43, 130.95, 130.86, 129.66, 121.98, 121.94, 119.46, 119.26, 116.36, 116.14, 40.46, 31.73, 30.08, 28.98, 26.86, 22.56, 14.03; Anal. Calcd for $\text{C}_{22}\text{H}_{25}\text{FN}_4\text{O}_2$: C, 66.65; H, 6.36; N, 14.13. Found: C, 66.82; H, 6.28; N, 14.22.

4.6.4. 1-(3-Dodecyl)-3-(4-(4-fluorophenyl)-1,2,5-oxadiazol-3-yl)phenylurea (**16j**)

Yield 70%; mp = 82–84 °C; TLC R_f = 0.34 (*n*-Hexane: Ethyl acetate, 7:3); IR (KBr, cm^{-1}): 3298, 2960, 1638, 1572, 1402, 1305, 1242, 990, 821; ^1H NMR: δ 8.62 (bs, 1H, NH), 7.9 (bs, 1H, NH), 7.2–7.4 (m, 8H, Ar-H), 3.1–3.3 (m, 2H, NHCH_2), 1.3–1.5 (m, 20H, CH_2), 0.9–1.02 (t, 3H, CH_3); Anal. Calcd for $\text{C}_{27}\text{H}_{35}\text{FN}_4\text{O}_2$: C, 69.50; H, 7.56; N, 12.01. Found: C, 69.37; H, 7.72; N, 12.14.

5. Biological activity

5.1. In vitro screening of the test compounds for SOAT inhibition

The biological activity of the test compounds for inhibition of SOAT was performed by the method described by Gandhi et al. [31] The SOAT assay mixture consisted of potassium phosphate buffer (0.1 M), BSA (5 mg/ml), microsomal protein (200 μg) and cholesterol solubilized in 45% w/v hydroxypropyl β -cyclodextrin (2 mM). Final reaction volume was made upto 850 μl with the help of 0.1 M potassium phosphate buffer. Vehicle, test compounds or the standard SOAT inhibitor (avasimibe, sigma) were added at this point (final volume NMT 10 μl) and incubated for 15 min to allow proper binding of the inhibitor with the SOAT enzymes. The reaction was initiated by the addition of 200 μM oleoyl CoA and allowed to proceed for 10 min at 37 °C. The reaction was terminated by the addition of 6 ml of a solution of chloroform-methanol (2:1, v/v) to the reaction mixture. The biphasic mixture was shaken in a separating funnel and both the phases were allowed to separate. The lower organic phase was collected and evaporated to dryness under a stream of N_2 gas. The residue was then re-dissolved in 500 μl of chloroform-methanol (2:1, v/v) and a volume of 25 μl from this solution was spotted on TLC plates for quantification. Each sample was applied to the TLC plates at least in triplicate. Activities of the compounds were determined by regression analysis of the spot areas determined by HPTLC (Camag, Switzerland) for cholesteryl oleate.

5.2. Poloxamer-407 induced lipoprotein lipase inhibition assay

Poloxamer-407 induced lipoprotein lipase inhibition was used to determine the changes in glyceride levels by the test compounds. Poloxamer-407 was procured as a generous gift sample from Wockhardt Ltd., Aurangabad, India. Avasimibe was purchased from Sigma Aldrich, St. Louis, MO, USA. Triglyceride estimation was performed by using commercial kits as per the manufacturer's protocol (GPO-PAP method, Coral Clinical Systems, Vapi, India).

Experiments were performed on healthy adult Wistar rats (20–24 weeks; 250–350 g). Baseline triglyceride levels were estimated in serum samples of all animals using the commercial kit on Day 0. Vehicle, test compounds (20 mg/kg) or avasimibe (20 mg/kg) suspended in 0.5% sodium CMC were administered on Day 1 by oral gavage in fasted animals. Four hours after the administration, lipoprotein lipase inhibitor Poloxamer-407 (1000 mg/kg), (prepared

as a 10% solution in 0.9% NaCl) was administered intraperitoneally. On Day 2, blood samples were withdrawn to estimate serum triglyceride levels. Results were analyzed to determine fold-changes in triglyceride levels over the test period of 24 h.

5.3. Evaluation of the effect of compound (**12d**) on lipid profile in animal model of diet-induced atherogenesis

The studies were performed on adult male Wistar rats (12–16 weeks old; 250–300 g). All the animals received drinking water *ad libitum*. Atherogenic diet [with or without compound (**12d**)] was made available to all the animals *ad libitum*. Compound (**12d**) was admixed in the desired concentration in the atherogenic diet on the basis of weekly food intake of the animals. Rats were housed in polypropylene cages with 12 h light/12 h dark cycles with temperature and humidity maintained at 23 ± 2 °C and 30–60% RH respectively. All experimental protocols described in the present study were approved by the Institutional Animal Ethics Committee (IAEC) of Pharmacy Department, The Maharaja Sayajirao University of Baroda with permission from Committee for the Purpose of Control and Supervision of Experiments on Animals (CPCSEA; MSU/PHARM/IAEC/2011–2013/01), Ministry of Environment, Forests and Climate Change, Government of India.

5.4. Preparation of atherogenic diet

The composition of the diet was as follows: cholesterol (2%), coconut oil (1%), cholic acid (1%), propylthiouracil (0.5%), casein (16.5%), powdered chow and hydroxypropyl cellulose (HPC) as binder (q.s. to 100%). After accurately weighing all the ingredients casein, cholic acid and propylthiouracil were ground in a mortar pestle until a homogenous solid mixture was formed. This dry mixture was added to a large vessel and mixed with required amount of powdered chow. Next, cholesterol was dissolved in appropriate volume of diethyl ether and this ethereal solution was properly mixed with the powder mass. The ether was allowed to evaporate for 2–3 h. Once the solvent got evaporated, required amount of coconut oil was mixed properly. For every kilogram of diet to be prepared, 800 ml of 1% HPC solution (prepared by stirring HPC in distilled water for about half an hour) was added at once to the dry mass and vigorously kneaded to evenly mix the ingredients. The consistency achieved was such that the lumps formed were neither crumbled nor too sticky. The lumps were hand cured to form suitably shaped masses which looked like pelleted chow. The final pellets were dried overnight in a hot-air oven at 45–50 °C. This step improves long term storage and prevents growth of microorganisms in the lumps. The pellets were stored in a perforated bag at 2–8 °C for not more than 7 days.

5.5. Experimental protocol

The animals were randomized into 3 groups of 6 animals each. The groups were as follows: 1. Progression Control group received atherogenic diet only, 2. Treatment Group I received atherogenic diet containing compound (**12d**) in such a way that the final daily dose of **12d** was 10 mg/kg, 3. Treatment Group II received atherogenic diet containing compound (**12d**) in such a way that the final daily dose of **12d** was 30 mg/kg. The study protocol is represented pictorially in Fig. 10.

All the blood samples were allowed to clot at room temperature for 15 min and centrifuged at $800 \times g$ for 15 min at 25 °C. The supernatant serum was collected and subjected to biochemical estimation for total cholesterol, triglycerides and HDL-C using commercially available diagnostic test kits. Other parameters like VLDL, LDL-C and atherogenesis index were derived by formulae on

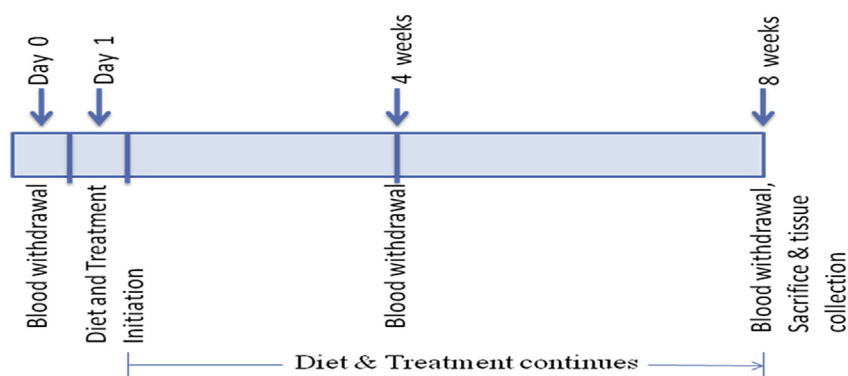


Fig. 10. Pictorial representation of the study protocol to see the effect of compound (**12d**) on lipid profile and related parameters in diet induced atherogenesis in rats.

the basis of these values. Towards the terminal stage of the study, animals were humanely sacrificed after blood sampling and thoracic aortae and aortic roots were carefully dissected.

5.6. *En face* lipid staining

It is a well known fact that the site of atherogenesis is unpredictable along the length of the thoracic aorta hence the thoracic aortae were subjected to *en face* staining with Sudan red IV solution (5 mg/ml in 70% isopropyl alcohol, vortexed and filtered). Thoracic aortae were isolated and cleaned of peri-adventitious tissue as it stains heavily with Sudan red IV. Care was taken to prevent damage to intima as lipid deposits might be dislodged upon mishandling. The aortae were split from the lumen to give strips. The strips were pinned to a white plate and immersed in Sudan red IV solution at 37 °C for 45 min. After this maneuver, the samples were destained for 10 min in 40% isopropyl alcohol. The stained tissue was photographed using a digital camera and images were analyzed using NIH (USA) image analysis software, ImageJ (ver. 1.43u, written by Wayne Rasband). Gross extent of atherosclerosis within the thoracic aorta was calculated by estimating the percent lesion area as compared to the total area. Data obtained were subjected to statistical analysis.

5.7. Luminal lipid plaque identification

The aortic roots were immediately washed with ice-cold PBS, cleared of surrounding adventitious fat, carotid connections were severed and immersed in 10% buffered formalin for cryosectioning. At the time of sacrifice, liver lobes were also removed to serve as support while sectioning the aortic roots. A small cavity was formed into the pith of the liver and one end of the aortic root was inserted inside the cavity. This whole lobe was now mounted on a chuck and put inside the sectioning instrument. The tissue was allowed to freeze for about 15–20 min and then the chuck was placed near the blade-rotor assembly. The blade was moved by the rotor to give a slicing motion and the sections were collected on a slide. The sections easily stick on the slide as soon as the slides are brought to room temperature due to the proteins in the section. The sections were stained with Sudan red IV solutions (5 mg/ml in 70% isopropyl alcohol, vortexed and filtered). The slides were put inside a coplin jar filled with Sudan red IV solution. The jar was incubated in a water bath at 37 °C for 45 min. The slides were then destained for 10 min in 40% isopropyl alcohol, cleaned after removing, observed at 10× magnification and photographed.

5.8. Statistical analysis

For all the studies, $n = 6$, except for *en face* staining, where $n = 3$. The data were presented in the form of mean \pm SEM. The results were compared by one-way ANOVA. Bonferroni's multiple comparisons were employed as the *post hoc* tests wherever required. All the statistical analyses were performed using Graphpad Prism, San Diego, CA, USA (Ver. 05). Results were considered to be statistically significant when $P < 0.05$.

5.9. Computational studies

5.9.1. Development of 3D-models of SOAT receptors

The MBOAT conserved domain of SOAT-1 was constructed by using I-TASSER [55–57]. Structurally similar proteins' folds were first identified from the PDB by multiple threading approach LOMETS. Continuous fragments excised from the PDB templates were reassembled into full-length models by replica-exchange Monte Carlo simulations with the threading of unaligned regions (mainly loops) built by *ab initio* modeling. Fragment assembly simulation was performed again starting from the SPICKER (near native model selection algorithm) cluster centroids, where the spatial restraints collected from the LOMETS templates and the PDB structures by TM-align were used to guide the simulations. The purpose of the second iteration was to remove the steric clash as well as to refine the global topology of the cluster centroids. The decoys generated in the second simulations were then clustered and the lowest energy structures were selected. The final full-atomic models were obtained by REMO which built the atomic details from the selected I-TASSER decoys through optimization of the hydrogen-bonding network.

5.9.2. Development of pharmacophore based 3D-QSAR model and docking studies

To develop a pharmacophore based 3D-QSAR model of SOAT inhibitors, a set of 32 SOAT inhibitors reported in this paper were used. PHASE was used to develop pharmacophore and 3D-QSAR models. Activity data and a given hypothesis in combination create a 3D-QSAR model which is able to recognize significant aspects of the molecular structures that govern the activity. All the 3D structures were drawn in MAESTRO and were minimized with default force field. In the beginning, conformations for all the molecules were searched through a combination of Monte-Carlo multiple minimum (MCM)/Low mode (LMOD) with a maximum number of 250 conformations per structure and 100 steps of minimization. A pharmaset was defined by setting a threshold values of $1/\log IC_{50} \geq 5.105$ for the 'actives' and $1/\log IC_{50} < 4.496$ for

the 'inactives'. PHASE presents a standard set of six pharmacophore features, namely hydrogen bond acceptor (A), hydrogen bond donor (D), hydrophobic (H) group, negatively ionizable (N) group, positively ionizable (P) group and aromatic ring (R). From the data set many hypotheses were developed, each having five pharmacophoric features. The generated common pharmacophore hypotheses were checked by scoring alignment of the 'actives' against a reference ligand by using default settings for 'Score Actives' to identify the pharmacophores from each box that resulted into the best alignment of the active ligands. The hypotheses were ranked according to the survival values for the 'active' and 'inactive' compounds.

Further, the developed pharmacophore model was studied with an atom based 3-D-QSAR model. In the atom-based 3D-QSAR, a molecule is treated as a set of overlapping van der Waals spheres. The van der Waals models of the aligned training set molecules were positioned in a regular grid of cubes, with each cube allotted zero or more 'bits' to account for the diverse types of atoms in the training set that occupy the cube. This illustration gives rise to binary-valued occupation patterns that can be used as independent variables to create partial least-squares 3D-QSAR models.

Molecular docking studies were performed using Glide (Schrodinger 2009). Glide performs grid-based ligand docking and explores favorable interactions between one or more small molecules i.e. ligands, and a larger receptor/enzyme molecule, a protein. Glide provides three levels of docking precision: high-throughput virtual screening (HTVS); standard precision (SP) and extra precision (XP). The ligand structures were built within Maestro using the Build module and a single low energy conformation search was performed for molecules under study using OPLS_2005 force field at physiological pH condition using LigPrep module of Schrödinger. Docking calculations were executed in XP mode with the active site of the receptor/enzyme structure.

Appendix A. Supplementary data

Supplementary data related to this article can be found at <http://dx.doi.org/10.1016/j.ejmech.2017.02.038>.

References

- [1] W.B. Kannel, W.P. Castelli, T. Gordon, P.M. McNamara, Serum cholesterol, lipoproteins, and the risk of coronary heart disease. The Framingham study, *Ann. Intern. Med.* 74 (1971) 1–12.
- [2] S.M. Grundy, G.J. Balady, M.H. Criqui, G. Fletcher, P. Greenland, L.F. Hiratzka, N. Houston-Miller, P. Kris-Etherton, H.M. Krumholz, J. LaRosa, I.S. Ockene, T.A. Pearson, J. Reed, R. Washington, S.C. Smith, Primary prevention of coronary heart disease: guidance from framingham, *Circulation* 97 (1998) 1876–1887.
- [3] E. Vassiliadis, N. Barascuk, M.A. Karsdal, Atherofibrosis - a unique and common process of the disease pathogenesis of atherosclerosis and fibrosis - lessons for biomarker development, *Am. J. Transl. Res.* 5 (2013) 1–14.
- [4] E. Falk, Pathogenesis of atherosclerosis, *J. Am. Coll. Cardiol.* 47 (2006) C7–C12.
- [5] P.R. Kamstrup, A. Tybjaerg-Hansen, R. Steffensen, B.G. Nordestgaard, Genetically elevated lipoprotein (a) and increased risk of myocardial infarction, *JAMA* 301 (2009) 2331–2339.
- [6] T.Y. Chang, C.C. Chang, N. Ohgami, Y. Yamauchi, Cholesterol sensing, trafficking, and esterification, *Annu. Rev. Cell Dev. Biol.* 22 (2006) 129–157.
- [7] I. Tabas, Consequences of cellular cholesterol accumulation: basic concepts and physiological implications, *J. Clin. Invest.* 110 (2002) 905–911.
- [8] T. Chang, B. Li, C.Y. Catherine, Y. Urano, Acyl-coenzyme A: cholesterol acyltransferases, *Am. J. Physiol. Endocrinol. Metab.* 297 (2009) E1–E9.
- [9] D.G. Karalis, Intensive lowering of low-density lipoprotein cholesterol levels for primary prevention of coronary artery disease, *Mayo Clin. Proc.* 84 (2009) 345–352.
- [10] a) J. Shepherd, S.M. Cobbe, I. Ford, C.G. Isles, A.R. Lorimer, P.W. MacFarlane, J.H. McKillop, C.J. Packard, Prevention of coronary heart disease with pravastatin in men with hypercholesterolemia. West of Scotland Coronary Prevention Study Group, *N. Engl. J. Med.* 333 (1995) 1301–1307; b) M.J. Chapman, J.K. Stock, H.N. Ginsberg, PCSK9 inhibitors and cardiovascular diseases: heralding a new therapeutic era, *Curr. Opin. Lipidol.* 26 (2015) 511–520; c) B.A. Golomb, M.A. Evans, Statin adverse effects: a review of the literature and evidence for a mitochondrial mechanism, *Am. J. Cardiovasc. Drugs* 8 (2008) 373–418; d) A. Marcello, P. Giovanni, Treating statin-intolerant patients, *Diabetes Metab. Syndr. Obes.* 4 (2011) 155–166.
- [11] A.T. Pearson, I. Laurora, H. Chu, S. Kafonek, The lipid treatment assessment project (L-TAP): a multicenter survey to evaluate the percentages of dyslipidemic patients receiving lipid-lowering therapy and achieving low-density lipoprotein cholesterol goals, *Arch. Intern. Med.* 160 (2000) 459–467.
- [12] T.C. Rideout, S.V. Harding, P.J. Jones, M.Z. Fan, Guar gum and similar soluble fibers in the regulation of cholesterol metabolism: current understandings and future research priorities, *Vasc. Health Risk Manag.* 4 (2008) 1023–1033.
- [13] I. Ikeda, Factors affecting intestinal absorption of cholesterol and plant sterols and stanols, *J. Oleo Sci.* 64 (2015) 9–18.
- [14] K.R. Norum, A.C. Lilljeqvist, P. Helgerud, E.R. Normann, A. Mo, B. Selbekk, Esterification of cholesterol in human small intestine: the importance of acyl-CoA: cholesterol acyltransferase, *Eur. J. Clin. Invest.* 9 (1979) 55–62.
- [15] J.G. Heider, C.E. Pickens, L.A. Kelly, Role of acyl CoA:cholesterol acyltransferase in cholesterol absorption and its inhibition by 57-118 in the rabbit, *J. Lipid. Res.* 24 (1983) 1127–1134.
- [16] F.J. Field, Intestinal cholesterol esterase: intracellular enzyme or contamination of cytosol by pancreatic enzymes, *J. Lipid. Res.* 25 (1984) 389–399.
- [17] K.E. Suckling, E.F. Stange, Role of acyl Co-A: cholesterol acyl transferase in cellular cholesterol metabolism, *J. Lipid Res.* 26 (1985) 647–671.
- [18] P. Helgerud, K. Saarem, K.R. Nonm, Acyl-CoA: cholesterol acyltransferase in human small intestine: its activity and some properties of enzymic action, *J. Lipid. Res.* 22 (1981) 271–277.
- [19] G. Vahouny, V. Falwal, C.R. Treadwell, Factor's facilitating cholesterol absorption from the intestine via lymphatic pathways, *Am. J. Physiol.* 188 (1957) 742–746.
- [20] N.D. Vaziri, K.H. Liang, ACAT inhibition ameliorates proteinuria, hyperlipidemia, lecithin-cholesterol acyltransferase, SRB-1 and low-density lipoprotein receptor deficiencies in nephritic syndrome, *Circulation* 110 (2004) 419–425.
- [21] C. Ta-Yuan, Li. Bo-Liang, C.Y. Chang, Y. Urano, Acyl-coenzyme A: cholesterol acyltransferases, *Am. J. Physiol. Endocrinol. Metab.* 297 (2009) E1–E9.
- [22] E.F. Largis, C.H. Wang, V.G. Davies, S.A. Schaffer, CL 277,082 : a novel inhibitor of ACAT-catalyzed cholesterol esterification and cholesterol absorption, *J. Lipid. Res.* 30 (1989) 681–690.
- [23] T.A. Bell, J.M. Brown, M.J. Graham, K.M. Lemonidis, R.M. Croke, L.L. Rudel, Liver-specific inhibition of acyl-coenzyme a: cholesterol acyltransferase 2 with antisense oligonucleotides limits atherosclerosis development in apolipoprotein B100-only low-density lipoprotein receptor-/-mice, *Arterioscler. Thromb. Vasc. Biol.* 26 (2006) 1814–1820.
- [24] P. Pal, H. Gandhi, R. Giridhar, M.R. Yadav, ACAT inhibitors: the search for novel cholesterol lowering agents, *Mini. Rev. Med. Chem.* 13 (2013) 1195–1219.
- [25] T. Ohshiro, T. Hiroshi, Acyltransferase inhibitors: a patent review (2010–present), *Expert Opin. Ther. Pat.* 25 (2015) 145–158.
- [26] S.E. Nissen, E.M. Tuzcu, H.B. Brewer, I. Sipahi, S.J. Nicholls, P. Ganz, L.M. Wisniewski, J.J. Hanyok, L.M. Kassalow, Effect of ACAT inhibition on the progression of coronary atherosclerosis, *N. Engl. J. Med.* 354 (2006) 1253–1263.
- [27] M.C. Meuwese, E. Groot, R. Duivenvoorden, M.D. Trip, L. Ose, F.J. Maritz, D.C. Basart, J.J. Kastelein, R. Habib, M.H. Davidson, A.H. Zwiderman, L.R. Schwach, E.A. Stein, ACAT inhibition and progression of carotid atherosclerosis in patients with familial hypercholesterolemia: the captivate randomized trial, *JAMA* 301 (2009) 1131–1139.
- [28] D. Vries, V.G. Largis, E.E. Miner, T.G. Shepherd, R.G. Upeslachs, Potential antiatherosclerotic agents. 4. [(Functionalized-alkyl)amino]benzoic acid analogs of cetaben, *J. Med. Chem.* 26 (1983) 1411–1421.
- [29] M.P. Giovannoni, V.P. Piaz, B.M. Kwon, M.K. Kim, Y.K. Kim, L. Toma, D. Barlocco, F. Bernini, M. Canavesi, 5,6-Diphenylpyridazine derivatives as ACAT inhibitor, *J. Med. Chem.* 44 (2001) 4292–4295.
- [30] a) S.T. Shirude, P. Patel, R. Giridhar, M.R. Yadav, An efficient and time saving microwave-assisted selenium dioxide oxidation of 1,2-diarylethanones, *Indian J. Chem.* 45B (2006) 1080–1085; b) R. Ramajayam, R. Giridhar, M.R. Yadav, R. Balaraman, H. Djaballah, D. Shum, C. Radu, Synthesis, antileukemic and antiplatelet activities of 2,3-diaryl-6,7-dihydro-5H-1,4-diazepines, *Eur. J. Med. Chem.* 43 (2008) 2004–2010.
- [31] H. Gandhi, P. Pal, R. Giridhar, M.R. Yadav, An HPTLC method for quantification of cholesteryl esters from human plasma and rat liver microsomes, *Biomed. Chrom.* 28 (2014) 583–588.
- [32] T. Kimura, Y. Takase, K. Hayashi, H. Tanaka, I. Ohtsuka, T. Saeki, M. Kogushi, T. Yamada, T. Fujimori, Structure-activity relationship of N-[2-(dimethylamino)-6-[3-(5-methyl-4-phenyl-1H-imidazol-1-yl)propoxy]phenyl]-N'-phenylurea and analogs. Novel potent inhibitors of acyl-CoA: cholesterol O-acyltransferase with antiatherosclerotic activity, *J. Med. Chem.* 36 (1993) 1630–1640.
- [33] T. Kumazawa, H. Harakawa, H. Fukui, S. Shirakura, E. Ohishi, K. Yamada, N-(1-phenyl-2-benzimidazolyl)-N'-phenylurea derivatives as potent inhibitors of acyl coa: cholesterol acyltransferase (ACAT), *Bioorg. Med. Chem. Lett.* 5 (1995) 1829–1832.
- [34] B.K. Trivedi, A. Holmes, T.S. Purchase, A.D. Essenburg, K.L. Hamelchle, B.R. Krause, M.S. Hes, R.L. Stanfield, A series of conformationally and sterically constrained analogs of N-phenyl-N'-aralkylurea ACAT inhibitors, *Bioorg. Med. Chem. Lett.* 5 (1995) 2229–2234.

- [35] A. Gelain, I. Bettinelli, D. Barlocco, B. Kwon, T. Jeong, K. Im, L. Legnani, L. Toma, Ureidopyridazine derivatives as acyl-CoA: cholesterol acyltransferase inhibitors, *Sci. Pharm.* 74 (2006) 85–97, 74.
- [36] S. Asano, H. Ban, K. Kino, K. Ioriya, M. Muraoka, Novel 1,4-diarylpiperidine-4-methylureas as anti-hyperlipidemic agents: dual effectors on acyl-CoA: cholesterol-O-acyltransferase and low-density lipoprotein receptor expression, *Bioorg. Med. Chem. Lett.* 19 (2009) 1062–1065.
- [37] M.A. Dominick, W.A. Bobrowski, J.R. Macdonald, A.W. Gough, Morphogenesis of a zone-specific adrenocortical cytotoxicity in Guinea pigs administered PD 132301-2, an inhibitor of acyl-CoA: cholesterol acyltransferase, *Toxicol. Pathol.* 21 (1993) 54–62.
- [38] H. Tawada, M. Harcourt, N. Kawamura, Novel acyl-CoA: cholesterol acyltransferase inhibitors. Synthesis and biological activity of 3-quinolyurea derivatives, *J. Med. Chem.* 37 (1994) 2079–2084.
- [39] G. Llaverrias, J.C. Launga, M. Algret, Pharmacology of the ACAT inhibitor avasimibe (CI-1011), *Cardiovasc. Drug Rev.* 21 (2003) 33–50.
- [40] T.P. Johnston, W.K. Palmer, Mechanism of poloxamer 407-induced hypertriglyceridemia in the rat, *Biochem. Pharmacol.* 46 (1993) 1037–1042.
- [41] T.Y. Chang, C.C. Chang, N. Ohgami, Y. Yamauchi, Cholesterol sensing, trafficking, and esterification, *Annu. Rev. Cell. Dev. Biol.* 22 (2006) 129–157.
- [42] R.E. Temel, L. Hou, L.L. Rudel, ACAT2 stimulates cholesteryl ester secretion in apoB-containing lipoproteins, *J. Lip. Res.* 48 (2007) 1618–1627.
- [43] K. Aragane, J. Kusunoki, T. Kitamine, Effects of F-1394, an acyl-CoA: cholesterol acyltransferase (ACAT) inhibitor, on ACAT activity in HepG2 cells and on hepatic secretion of lipids in Triton WR-1339-induced hyperlipidemic rats: possible role of hepatic ACAT in very low density lipoprotein secretion, *Jpn. J. Pharmacol.* 76 (1998) 309–312.
- [44] T. Uchida, K. Aoyama, T. Watanbe, Relationship between bioavailability and hypocholesterolemic activity of YM17E, an inhibitor of ACAT, in cholesterol-fed rats, *Atherosclerosis* 137 (1998) 97–106.
- [45] T.N. Tulenko, A.E. Summer, The physiology of lipoproteins, *J. Nucl. Cardiol.* 9 (2002) 638–649.
- [46] a) J. Kusunoki, K. Aragane, T. Kitamine, Hypocholesterolemic action and prevention of cholesterol absorption via the gut by f-1394, a potent acyl-coa: Cholesterol acyltransferase (ACAT) inhibitor, in cholesterol diet-fed rats, *Jpn. J. Pharmacol.* 69 (1995) 53–60;
b) R. Arakawa, S. Abe-Dohmae, M. asai, J. I. Ito, S. Yokoyama, Involvement of caveolin-1 in cholesterol enrichment of high density lipoprotein during its assembly by apolipoprotein and THP-1 cells, *J. Lip. Res.* 41 (2000) 1952–1962.
- [47] a) W.T. Friedewald, R.I. Levy, D.S. Fredrickson, Estimation of the concentration of low-density lipoprotein cholesterol in plasma, without use of the preparative ultracentrifuge, *Clin. Chem.* 18 (1972) 499–502;
b) P.A. Luz, D. Favarrato, J.R.F. Junior, P. Lemos, A.C.P. Chagas, High ratio of triglycerides to HDL-cholesterol predicts extensive coronary disease, *Clinics* 63 (2008) 427–432.
- [48] T. Oshiro, M. Muraoka, K. Ioriya, Pyripropene A, an Acyl-Coenzyme A: cholesterol acyltransferase 2-selective inhibitor, attenuates hypercholesterolemia and atherosclerosis in murine models of hyperlipidemia, *Arterioscler. Thromb. Vasc. Biol.* 31 (2011) 1108–1115.
- [49] K. Lee, S. Cho, J.H. Lee, Synthesis of a novel series of 2-alkylthio substituted naphthoquinones as potent acyl-CoA: cholesterol acyltransferase (ACAT) inhibitors, *Eur. J. Med. Chem.* 62 (2013) 515–525.
- [50] D.G. Robertson, M.A. Breider, M.A. Milad, Preclinical safety evaluation of avasimibe in beagle dogs: an acat inhibitor with minimal adrenal effects, *Toxicol. Sci.* 59 (2001) 324–334.
- [51] B.D. Roth, ACAT inhibitors: evolution from cholesterol-absorption inhibitors to antiatherosclerotic agents, *Drug Discov. Today* 3 (1998) 19–25.
- [52] H. Yagyu, T. Kitamine, J.I. Osuga, Absence of ACAT-1 attenuates atherosclerosis but causes dry eye and cutaneous xanthomatosis in mice with congenital hyperlipidemia, *J. Biol. Chem.* 275 (2000) 21324–21330.
- [53] M. Accad, S.J. Smith, D.L. Newland, D.A. Sanan, L.E. King, M.F. Linton, S. Fazio, R.J. Farese, Massive xanthomatosis and altered composition of atherosclerotic lesions in hyperlipidemic mice lacking acyl CoA:cholesterol acyltransferase 1, *J. Clin. Invest.* 105 (2000) 711–719.
- [54] C.W. Joyce, G.S. Shelness, M.A. Davis, R.G. Lee, K. Skinner, R.A. Anderson, L.L. Rudel, ACAT1 and ACAT2 membrane topology segregates a serine residue essential for activity to opposite sides of the endoplasmic reticulum membrane, *Mol. Biol. Cell.* 11 (2000) 3675–3687.
- [55] J. Yang, R. Yan, A. Roy, D. Xu, J. Poisson, Y. Zhang, The I-TASSER Suite: protein structure and function prediction, *Nat. Methods* 12 (2015) 7–8.
- [56] A. Roy, A. Kucukural, Y. Zhang, I-TASSER: a unified platform for automated protein structure and function prediction, *Nat. Protoc.* 5 (2010) 725–738.
- [57] Y. Zhang, I-TASSER server for protein 3D structure prediction, *BMC Bioinforma.* 9 (2008) 40–47.
- [58] S.L. Dixon, A.M. Smondyrev, S.N. Rao, A novel approach to pharmacophore modeling and 3D database searching, *Chem. Biol. Drug Des.* 67 (2006) 370–372.
- [59] A.M. Kanhed, V.P. Zambre, V.A. Pawar, M.K. Sharma, R. Giridhar, M.R. Yadav, Structural requirements for imidazo [1, 2-*a*] pyrazine derivatives as Aurora A kinase inhibitors and validation of the model, *Med. Chem. Res.* 23 (2014) 5215–5223.
- [60] A.M. Kanhed, R.C. Dash, N. Parmar, T. Kumar, R. Giridhar, M.R. Yadav, Benzo[e] pyrimido[5,4-*b*][1,4]diazepin-6(11*H*)-one derivatives as Aurora A kinase inhibitors: LQTA-QSAR analysis and detailed systematic validation of the developed model, *Mol. Divers* 19 (2015) 965–974.